# NAVAL POSTGRADUATE SCHOOL
## Monterey, California

# THESIS

**RADIATION EFFECTS ON MULTI-JUNCTION SOLAR CELLS**

by

Tommy L. Fifer

December 2001

| | |
|---|---|
| Thesis Advisor: | Sherif Michael |
| Second Reader: | Ron Pieper |

**Approved for public release; distribution is unlimited.**

# Report Documentation Page

| Report Date | Report Type | Dates Covered (from... to) |
|---|---|---|
| 19 Dec 2001 | N/A | - |

| Title and Subtitle | | Contract Number |
|---|---|---|
| Radiation Effects on Multi-Junctions Solar Cells | | |
| | | **Grant Number** |
| | | **Program Element Number** |

| Author(s) | | Project Number |
|---|---|---|
| Fifer, Tommy L. | | |
| | | **Task Number** |
| | | **Work Unit Number** |

| Performing Organization Name(s) and Address(es) | Performing Organization Report Number |
|---|---|
| Naval Postgraduate School Monterey, California | |

| Sponsoring/Monitoring Agency Name(s) and Address(es) | Sponsor/Monitor's Acronym(s) |
|---|---|
| | **Sponsor/Monitor's Report Number(s)** |

**Distribution/Availability Statement**
Approved for public release, distribution unlimited

**Supplementary Notes**

**Abstract**

**Subject Terms**

| Report Classification | Classification of this page |
|---|---|
| unclassified | unclassified |

| Classification of Abstract | Limitation of Abstract |
|---|---|
| unclassified | UU |

**Number of Pages**
90

THIS PAGE INTENTIONALLY LEFT BLANK

| REPORT DOCUMENTATION PAGE | | | *Form Approved OMB No. 0704-0188* |
|---|---|---|---|
| Public reporting burden for this collection of information is estimated to average 1 hour per response, including the time for reviewing instruction, searching existing data sources, gathering and maintaining the data needed, and completing and reviewing the collection of information. Send comments regarding this burden estimate or any other aspect of this collection of information, including suggestions for reducing this burden, to Washington headquarters Services, Directorate for Information Operations and Reports, 1215 Jefferson Davis Highway, Suite 1204, Arlington, VA 22202-4302, and to the Office of Management and Budget, Paperwork Reduction Project (0704-0188) Washington DC 20503. | | | |
| **1. AGENCY USE ONLY** (*Leave blank*) | **2. REPORT DATE** December 2001 | **3. REPORT TYPE AND DATES COVERED** Master's Thesis | |
| **4. TITLE AND SUBTITLE**: Title (Mix case letters) Radiation Effects on Multi-junction Solar Cells | | | **5. FUNDING NUMBERS** |
| **6. AUTHOR(S) Fifer, Tommy L.** | | | |
| **7. PERFORMING ORGANIZATION NAME(S) AND ADDRESS(ES)** Naval Postgraduate School Monterey, CA 93943-5000 | | | **8. PERFORMING ORGANIZATION REPORT NUMBER** |
| **9. SPONSORING /MONITORING AGENCY NAME(S) AND ADDRESS(ES)** N/A | | | **10. SPONSORING/MONITORING AGENCY REPORT NUMBER** |
| **11. SUPPLEMENTARY NOTES** The views expressed in this thesis are those of the author and do not reflect the official policy or position of the Department of Defense or the U.S. Government. | | | |
| **12a. DISTRIBUTION / AVAILABILITY STATEMENT** Approved for public release; distribution is unlimited. | | | **12b. DISTRIBUTION CODE** |
| **13. ABSTRACT** (*maximum 200 words*) The GaInP$_2$/GaAs/Ge monolithic high efficiency triple junction cell is the state of the art multi-junction solar cell for space applications. Numerous labs have undertaken investigation into the stability of GaInP2/GaAs/Ge in response to electron radiation. Electron radiation experiments have shown that the degradation of GaInP$_2$/GaAs/Ge solar cells is mainly caused by a decrease of the short circuit current ($I_{SC}$). The investigation and interpretation of the damage mechanism from electron irradiation in Spectrolab's GaInP$_2$/GaAs/Ge triple junction cell is the purpose of this thesis. Current voltage characteristics were measured to establish beginning of life (BOL) parameters of the solar cells and the changes that occur due to irradiation (EOL). | | | |
| **14. SUBJECT TERMS** Solar Cell, Multi-junction solar cells, GaInP2/GaAs/Ge | | | **15. NUMBER OF PAGES** |
| | | | **16. PRICE CODE** |
| **17. SECURITY CLASSIFICATION OF REPORT** Unclassified | **18. SECURITY CLASSIFICATION OF THIS PAGE** Unclassified | **19. SECURITY CLASSIFICATION OF ABSTRACT** Unclassified | **20. LIMITATION OF ABSTRACT** UL |

THIS PAGE INTENTIONALLY LEFT BLANK

# RADIATION EFFECTS ON MULTI-JUNCTION SOLAR CELLS

Tommy L. Fifer
Lieutentant, United States Navy
B.S., Memphis State University, 1994

Submitted in partial fulfillment of the
requirements for the degree of

# MASTER OF SCIENCE IN ELECTRICAL ENGINEERING

from the

# NAVAL POSTGRADUATE SCHOOL
## December 2001

Author: _____
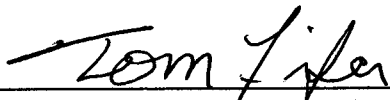
Tommy L. Fifer

Approved by: _____

Sherif Michael, Thesis Advisor

_____

Ron Pieper, Second Reader

_____
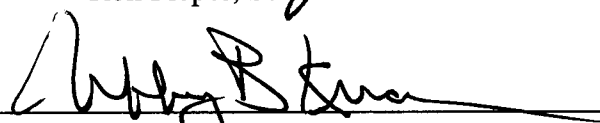
Jeffrey B. Knorr, Chairman
Department of Electrical and Computer Engineering

iii

THIS PAGE INTENTIONALLY LEFT BLANK

# ABSTRACT

The GaInP$_2$/GaAs/Ge monolithic high efficiency triple junction cell is the state of the art multi-junction solar cell for space applications. Numerous labs have undertaken investigation into the stability of GaInP2/GaAs/Ge in response to electron radiation. Electron radiation experiments have shown that the degradation of GaInP$_2$/GaAs/Ge solar cells is mainly caused by a decrease of the short circuit current ($I_{SC}$). The investigation and interpretation of the damage mechanism from electron irradiation in Spectrolab's GaInP$_2$/GaAs/Ge triple junction cell is the purpose of this thesis. Current voltage characteristics were measured to establish beginning of life (BOL) parameters of the solar cells and the changes that occur due to irradiation (EOL).

THIS PAGE INTENTIONALLY LEFT BLANK

# TABLE OF CONTENTS

# LIST OF FIGURES

THIS PAGE INTENTIONALLY LEFT BLANK

# LIST OF TABLES

THIS PAGE INTENTIONALLY LEFT BLANK

# ACKNOWLEDGMENTS

I would like to thank Professor Michael for his support in this research. I would also like to Thank Dan Sakoda for his patience and insight during the beginning phase of my thesis. Although the LINAC was my Albatross, I give thanks to Don Snyder for his assistance. The effort to get me "data" was appreciated.

Finally, I would like to thank my Patricia for her love and support throughout the entire thesis process

THIS PAGE INTENTIONALLY LEFT BLANK

# EXECUTIVE SUMMARY

The $GaInP_2$/GaAs/Ge monolithic high efficiency triple junction cell is the state of the art multi-junction solar cell for space applications. The purpose of this thesis is to investigate and interpret the displacement damage mechanisms Spectrolab's $GaInP_2$/GaAs/Ge experienced due to electron irradiation. Other electron radiation experiments have shown that the degradation of $GaInP_2$/GaAs/Ge solar cells is mainly shown as a decrease of the short circuit current ($I_{SC}$). Current voltage characteristics were performed to establish beginning of life (BOL) parameters of the solar cells and the changes that occur due to irradiation (EOL). The complete irradiation of the test cells was not accomplished because the LINAC is currently not operational. This summary will include a description of procedures that were accomplished.

The solar simulator used in this research was an Optical Radiation Corporation model SS-1000. The SS-1000 uses a xenon bulb that closely approximates the spectral distribution of sunlight under Air Mass Zero (AM0) conditions. AM0 is the spectral irradiance that solar cells experience in space. The entire simulation and test set-up consists of the SS-1000, a Hewlett-Packard programmable power supply (HP 6626A), vacuum assisted/ temperature controlled brass test block, and a personal computer with an HP-IB interface card running LABVIEW software. Figure 1 shows the experimental set-up.

Calibration of the SS-1000 was accomplished by adjusting the spectral intensity of the simulator to reproduce the characteristic values of the reference cell. The reference cell used was a GaInP2/GaAs/Ge cell manufactured by Spectrolab. The cell was chosen to match the spectrum of cells being investigated in this thesis.
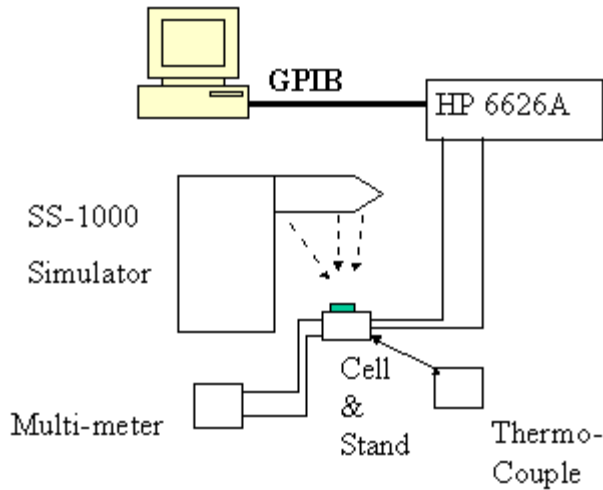
**Figure 1. Solar Simulation System.**

A Pentium based personal computer (PC) provided experiment control using the LabView™ Version 5.0 software. LabView™ is a virtual instrumentation program that allows precise control of the represented test instrument. The SS-1000 illuminates the cell under test. The test cell's output voltage and current were measured at each interval and stored in a data file. The characteristic current and voltage curves were generated from this data.

Analysis of current-voltage (IV) characteristics is the method that will be used to evaluate and interpret the radiation effects on Spectrolab's $GaInP_2$/GaAs/Ge triple-junction cell. Figure 2 shows a characteristic curve for a solar cell. The IV Curves were measured at (BOL) and after (EOL) irradiation. Solar cells are characterized by quantities extracted from the cells' current-voltage (IV) curve. Open circuit voltage ($V_{OC}$) is the threshold up to which the junction will power an electrical load. Short circuit current ($I_{SC}$) is the current value at zero bias. Maximum current and voltage ($I_m$, $V_m$) are the values for I and V when most power is delivered. The fill factor (FF) is a measure how efficient the power extraction is. The fill factor is defined as: FF= [$P_M$/($V_{OC}$ x $I_{SC}$)] x 100. The conversion efficiency, defined as: Efficiency= $P_M$/(135.3 x A). Where 135.3 mW/cm$^2$ is the solar constant at AM0 and A is the surface area of the cell in cm$^2$.
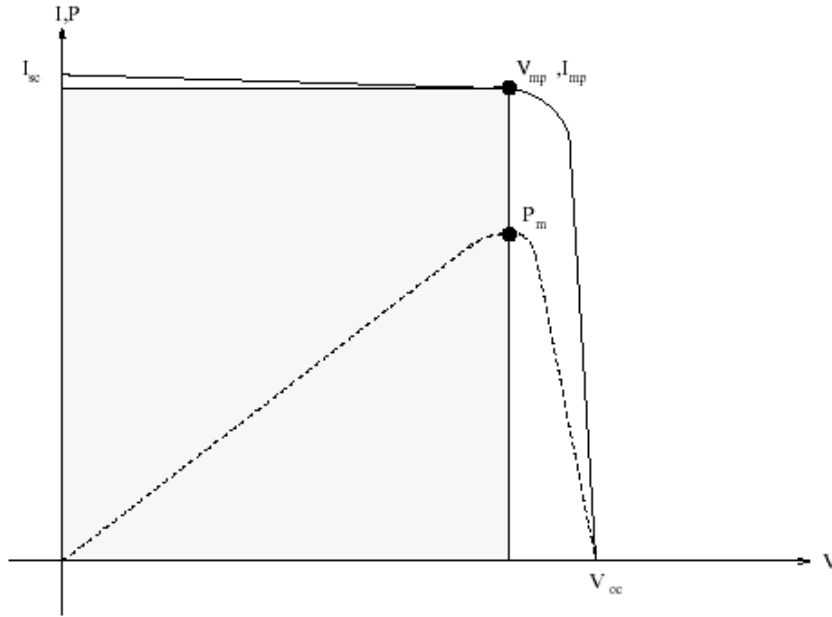
**Figure 2. Characteristic IV Curve.**

The NPS LINAC was used to simulate the electron radiation environment. The initial test plan was the cells were to be irradiated with 90 Mev electrons and total fluence of $1x10^{15}$ electrons/cm$^2$. The electrical characteristics were to be measured at intervals of $1x10^{14}$ electrons/cm$^2$ of irradiation. These characteristics were to be plotted as curves of electrical degradation vs fluence. Due to the LINAC malfunctioning, the irradiation was not completed. There was data for only one value of fluence at $5x10^{14}$ electrons/cm$^2$. The irradiation data is presented in Table 1. This type of degradation is representative of damage solar cells would experience when the cells transverse the outer Van Allen belt where the electrons energies are higher and more dynamic.

| $V_{OC1}$ (V) | $V_{OC2}$ (V) | Ratio | $I_{SC1}$ (mA/cm$^2$) | $I_{SC2}$ (mA/cm$^2$) | Ratio |
|---|---|---|---|---|---|
| 2.5748 | 2.4083 | .935 | 14.77124975 | 13.39375 | .906 |
| | | | | | |
| FF1 (%) | FF2 (%) | Ratio | η1 | η2 | Ratio |
| 86.48925 | 81.72 | .94 | 24.3 | 19.5 | .802 |

Table1. IV Test Results for BOL and EOL.

In order to make a conclusive determination concerning the degradation experienced the complete irradiation of the test cells must be completed. However this thesis does serve as a good reference for basic solar cell theory, multi-junction theory, and solar cell irradiation and test procedures.

THIS PAGE INTENTIONALLY LEFT BLANK

# I.  INTRODUCTION

In the 1980's, GaAs-based cells replaced silicon as the technology of choice for critical space missions requiring high operating power. GaAs radiation hardness led to this trend.  Optimization of the technology led to efficiencies around 18.5%.  Since the early 1990s, space photovoltaic (PV) power system requirements have increased by approximately 400%.   This is due to the growing complexity and length of the space missions and the worldwide proliferation of satellite-based communication systems.

Modern spacecraft such as NASA's Deep Space 1 (DS1) requires more electrical energy to run increasingly complicated and diversified payloads for the length of its mission.  Several communications satellites have been launched with a total power in excess of 40 kW. The high power allows for more transponders, which translate to higher performance.  Thus the system can support complex on-board activities such as digital signal processing.

The challenge for space PV power system designers is to create the space solar cell technology to generate the required power throughout the mission of the spacecraft or satellite.  The ideal space solar cell has the following characteristics:

- high efficiency because available area and weight are extremely limited.
- good radiation tolerance to damage from natural radiation belts, and possibly from man-made sources.
- temperature control since the only heat loss is by radiation.
- tolerance to extreme UV radiation, to atomic oxygen degradation (in LEO), and to electrostatic damage from charged particle build-up.
- robustness and high reliability, especially when exposed to many cycles of severe temperature excursions

Space PV power system designers have two options available to increase the power from solar arrays either they increase the total array area, or use solar cells with higher conversion efficiency.  The latter is the logical choice because the real estate allocated to space PV power systems is inherently small.  Multi-junction solar cells are the solution.

Multi-junction solar cells are multiple band-gap semiconductor devices that take advantage of the sun's broad spectrum.  The structure of the device is such that the

semiconductor materials are arranged in descending band-gap order.  Because of this arrangement, fewer incident photons are lost in the form heat resulting in a more efficient device. The commercially available multi-junction cells are made from III-V materials. However, there is increasing research on using II-VI materials. Figure I-1 shows a schematic of a multi-junction cell.
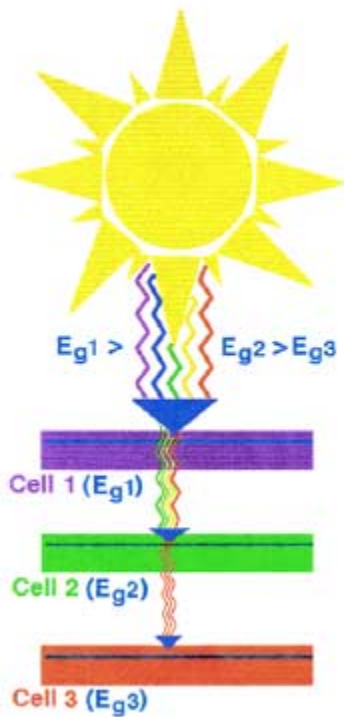


**Figure I-1.  A multi-junction device is a stack of individual single-junction cells in descending order of band gap (Eg) [From: Ref. 30: pg 2].**

The characteristics of space power solar cells were discussed.  The most critical characteristic is the radiation hardness of the device.  The space radiation environment degrades the long-term performance of the solar cell. Designers have to create a system whose end of life (EOL) power, the power after radiation degradation, still meet the minimum power requirement of the system at missions end.  So, it is critical that the radiation affects on the solar cell performance is understood.  This thesis will investigate the radiation effects on multi-junction solar cells.

Chapter II will discuss the radiation environment and its affects on solar cells. Chapter III describes the NPS Linear accelerator (LINAC), the radiation source used in this thesis.  Chapter IV examines the semiconductor physics of solar cells.  Chapter V

describes the multi-junction solar cell. Chapter VI is the experimental section that examines the radiation effects on the test cell, and Chapter VII is the conclusion.

THIS PAGE INTENTIONALLY LEFT BLANK

# II.  SPACE RADIATION ENVIRONMENT

## A.    INTRODUCTION

The radiation environment in space depends strongly on location, and is composed of a variety of particles with widely varying energies and states of ionization. For this discussion we will discuss the space environment in terms of the natural occurring space radiation (Van Allen belts, solar flares, and galactic cosmic rays) with the understanding that designers are aware of enhanced space environments.  Military satellites are susceptible to a nuclear enhanced space radiation environment.

Satellites often operate in the space environment for many years. As a result solar cells can sustain long-term exposure effects. The amount of exposure depends on their altitude, the nature and trajectory of the mission.

### 1.    Solar Wind.

The high temperature of the Sun's corona allows solar protons and electrons to gain enough velocity to escape the gravitational attraction of the sun. The continuous outward flow of hot protons and electrons is called the solar wind.   The solar wind causes the Earth's magnetic trapping region facing the sun to be hemispherical.  The solar wind affects the daylight side of Earth. Van Allen belts result when the Earth catches electrons and protons gyrating around magnetic field lines.

### 2.    Van Allen Radiation Belts.

The primary cause of degradation to solar cells is caused by repeated traversals of the Van Allen radiation belts. The radiation or van Allen belts are the trapping regions of high-energy charged particles surrounding the Earth. The inner belt is located between about 300-6400 km above earth in the equatorial plane.  It contains primarily protons with energies exceeding 10 MeV [Ref. 1 pg 5.1-5.9].  As a result of the offset between the Earth's geographical and magnetic axes, the inner belt reaches a minimum altitude of about 250 km above the Atlantic Ocean off the Brazilian Coast [Ref. 1 pg 5.1-5.9].  This region is called the South Atlantic Anomaly.

The outer belt contains mainly electrons with energies up to 10 MeV. It is produced by injection and energizing events following geomagnetic storms, which makes it much more dynamic than the inner belt (it is also subject to day-night variations). It has an equatorial distance of about 3 - 9 Earth Radii Re, with maximum for electrons above 1 MeV occurring at about X = 4 Re [Ref. 1 pg 5.1-5.9]. Figure II-1 depicts the Van Allen belts.
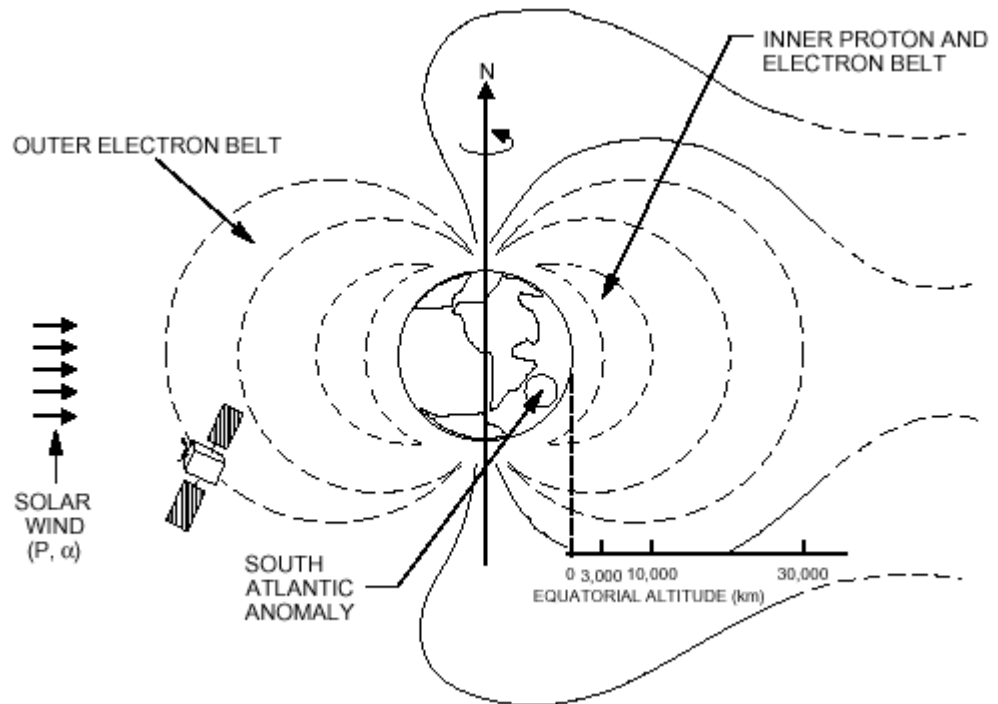


**Figure II-1. Schematic Diagram of the Earth's Van Allen Belts [From: Ref. 2: pg 203].**

### 3. Solar Flares

Solar flares are another important source of ionizing radiation particles particularly protons. Sunspot activity follows an approximate 11-year cycle. The sunspot activity does not necessarily result in significant solar flares. Solar flares can vary significantly in their proton energy spectrum. This, along with the inability to predict when a solar flare will occur, forces space system designers to use large estimates of potential flare activity [Ref. 2 pg 205].

### 4. Galactic Cosmic Rays

The third important source of radiation in the natural space environment is galactic cosmic rays (GCRs), consisting of mainly protons. These energetic particles (energies as high as 10 GeV/nucleon) originate outside the solar system. These heavy ions deposit large amounts of energy and their damage is proportional. It is important to note that ionization from GCR is a rare occurrence [Ref. 2 pg 205].

## B. RADIATION DAMAGE MECHANISM

Characterizing radiation damage mechanisms in a solar cell is extremely complex. Since the particles have mass, energy and possibly charge, they can interact in several ways with materials. The dominant interactions are [Ref. 1 pg 3.1-3.2]:

### 1. Inelastic Collisions With Atomic Electrons.

Incident energetic charged particles lose kinetic energy in the material. In such collisions, electrons experience a transition to an excited state (excitation) or to an unbound state (ionization).

### 2. Elastic Collisions With Atomic Nuclei.

Energetic charged particles may have coulombic reactions with the positive charge of the atomic nucleus through Rutherford scattering. In some cases the amount of energy transferred to the atom will displace it from its position in a crystalline lattice. This energetic displaced atom may in turn undergo similar collisions with other atoms of the material. If sufficient energy is transferred to displace an atom from its lattice site, that atom will probably be energetic enough to displace many other atoms.

### 3. Inelastic Collisions With Atomic Nuclei.

In this process, the energetic proton interacts with the nucleus and leaves the nucleus in an excited or activated state. The excited nucleus emits energetic nucleons and the recoiling nucleus is displaced from its lattice site. This recoiling nucleus in turn causes more displacements.

## C.    IONIZATION AND DISPLACEMENT DAMAGE

The discussion on damage mechanism clearly indicates that the major type of radiation damage of interest in solar cells is damage resulting from ionization and atomic displacement.

### 1.    Ionization Damage.

Ionization occurs when a charged particle imparts energy to an atom and excites a valence electron to the conduction band. As a result electron-hole pairs are created which affect majority and minority carrier concentrations in the cell.    If an electric field is present, some electrons and holes immediately recombine with other atoms or become trapped in lattice defect sites [Ref. 2: pg 211].

Another ionizing radiation affect is that it induces permanent interface traps. These traps can shift threshold voltages. They can also reduce carrier mobility, which affects device speeds [Ref. 2: pg 211].

Ionizing radiation reduces the transmittance in solar cell cover glasses.    Dark color centers develop from long-term effects. These color centers are the result of the ionized electron becoming trapped by impurity atoms in the cover glass.    These charge centers are relatively stable at room temperature [Ref 3].    Under normal circumstances, ionization itself does not impart any true damage to the structure of a solar cell. If the trapped charge could be removed, normal operation of the device would be reinstated.

### 2.    Displacement Damage

Elastic and inelastic collisions with atomic nucleues are the primary mechanism for displacement damage.  Displacement damage occurs when particles knock atoms out of their proper crystal lattice locations creating defects in the crystal structure.  These, defects are in the form of interstitials and vacancies.  Interstitials are displaced atoms in semi-stable postition in the crystal structure.  The pairing of the interstitial and vacancy is called Frenkel defects.  These defect sites introduce additional energy levels into the energy band gap of the semiconductor. The introduction of these states alters the electrical properties of the device through four mechanisms [Ref. 8]:

- generation of electron-hole pairs (leading to thermal dark current in detectors);

- recombination of electron-hole pairs (leading to reduction of minority carrier lifetime and effects);

- trapping of carriers, leading to loss in charge transfer efficiency (minority carrier trapping) or carrier removal (majority carrier trapping);

- compensation of donors or acceptors (also leading to carrier removal in some devices);

Figure II-2 shows the defect mechanisms. The overall affect of these additional states is the reduction in minority carrier lifetime in solar cells. If the minority lifetime is reduced then the photocurrent is reduced in the solar cell.
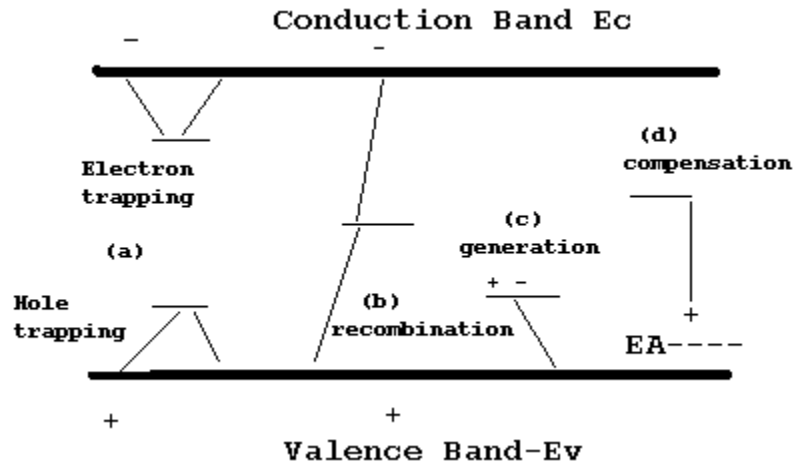


**Figure II-2. Four of the Primary mechanisms resulting crystal lattice defects: (a) Trapping, (b) recombination, (c) Generation, and (d) Compensation [From: Ref. 8].**

### a. Non-Ionizing Energy Loss (NIEL).

Displacement damage is defined in terms of energy deposited as Non-Ionizing Energy Loss (NIEL) with units of energy per unit mass (e.g. eV per $cm^2$/ gm). Since the induced damage is a function of the particle nature and energy, the Non-Ionizing Energy Loss (NIEL) is used as a parameter to correlate the effects observed in different radiation environments. When calculating the effect of such a broad particle spectrum, it is necessary to select a standard particle energy and assign to this a damage

effectiveness of unity. If the standard particle and energy chosen is 1 MeV electrons, then the functional damage due to a particle spectrum can be expressed in simple terms, using the unit equivalent 1 MeV electrons per cm$^2$ [Ref. 7].

## D.    MEASUREMENT OF RADIATION EFFECTS

From the discussion above, displacement damage has a direct affect on minority carrier lifetime. So, solar cell damage can be quantified in terms of the changes in the minority carrier lifetime. Chapter IV describes the inverse relationship of recombination rate to minority carrier lifetime. The result is that the following equation can be used to quantify radiation damage to solar cell.

$$\frac{1}{\tau} = \frac{1}{\tau_0} + \left( \frac{1}{\tau_e} + \frac{1}{\tau_p} \right) = \frac{1}{\tau_0} + \left( K_{\tau_e} \times \Phi_e \right) + \left( K_{\tau_p} \times \Phi_p \right) \tag{2.1}$$

Where $\tau$ is the minority carrier lifetime, $\tau_0$ is the initial minority carrier lifetime, $\tau_e$ is the minority carrier lifetime due to electron irradiation, $\tau_p$ is the minority carrier lifetime due to proton irradiation, $K_\tau$ is the damage coefficient (lifetime), and $\Phi$ is the radiation fluence [Ref. 1:pg 3-16]. This approach has its drawbacks. First and foremost, measuring the minority carrier lifetime is not practical. Although measuring the diffusion length is possible, correlating changes in diffusion length is not linear for electron and proton displacement damage. The standard approach to quantifying radiation damage is observing changes in the electrical parameters used to characterize solar cells: short circuit current ($I_{SC}$), open circuit voltage ($V_{OC}$), and maximum power ($P_{max}$). The following equations show the empirical relationship describing the changes in the electrical parameters.

$$I_{SC} = I_{SC}(0) - C\log\left(1 + \frac{\Phi}{\Phi_x}\right) \tag{2.2}$$

$$V_{OC} = V_{OC}(0) - K\log\left(1 + \frac{\Phi}{\Phi_x}\right) \tag{2.3}$$

$$P_{max} = P_{max}(0) - H \log\left(1 + \frac{\Phi}{\Phi_x}\right) \qquad (2.4)$$

Where C, K, and H are constants of proportionality, $\Phi_x$ represents the radiation fluence at which $I_{sc}$ starts to change to a linear function of the logarithm of the fluence, and $\Phi$ is the radiation fluence (#/cm$^{-2}$).

## E.    PREVIOUS IRRADIATION RESEARCH

Research has shown that the GaInP$_2$/GaAs/Ge triple-junction cell radiation performance is limited by the GaAs middle cell. This result was derived from comparing BOL quantum efficiency curves to EOL curves. BOL and EOL quantum efficiencies were integrated using the following formula to calculate $I_{SC}$. Quantum efficiency will be discussed briefly in chapter four. Figure II-2 shows the external quantum efficiencies of the GaInP2 and GaAs sub cells.

$$I_{SC} = q \int b_s(\text{E}) \, \text{QE(E)} dE \qquad (2.5)$$

Where $b_S$ is the incident photon flux of energy, E in the illuminating spectra, and QE is the quantum efficiency. The ratio of integrated current was 93% and 80% for the GaInP$_2$ and GaAs respectively. So it is clear that the GaAs cell is the limiting cell [Ref.1: pg 49]. The germanium (Ge) cell was not investigated because independent test showed that germanium's maximum achievable current is much greater than cell 1 or 2. Subsequent degradation would produce a relatively small change in quantum efficiency. Table II-2 shows the maximum achievable current for the sub-cells.
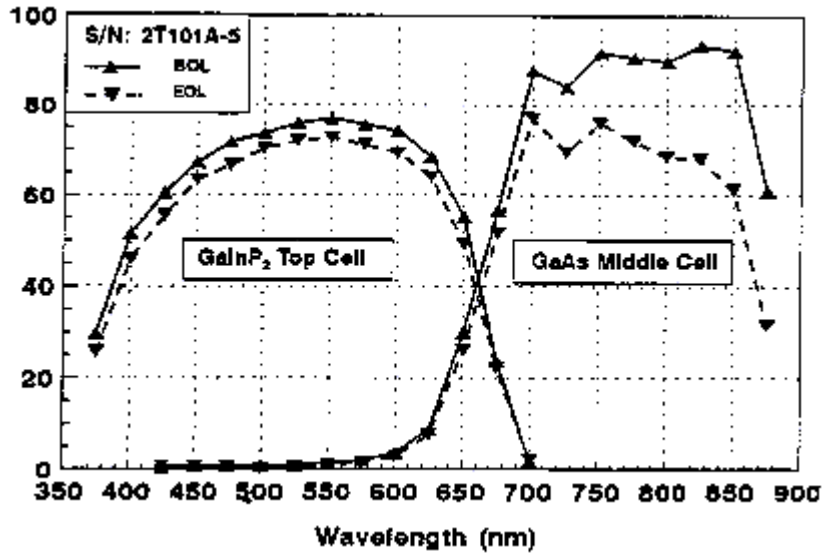
**Figure II-2. BOL&EOL External Quantum Efficiency of GaInP2/GaAs/Ge Triple junction cell [From: Ref. 26: pg 54].**

| Subcell | Maximum Achievable $J_{sc}$ (mA/cm$^2$) |
|---|---|
| 1.86 eV InGaP$_2$ | 22.1 |
| 1.42 eV GaAs | 15.6 |
| 0.66 eV Ge | 42.4 |

**Table II-1. Maximum achievable $J_{SC}$ for each subcell in an InGaP/GaAs/Ge triple junction Solar Cell [From: Ref. 24 pg 1].**

### 1. Relative Damage Coefficients.

There has been extensive research on Si and GaAs. Hence there are established relationships between NIEL and the damage coefficient. In the case of p-type Si and GaAs cells, the electron damage coefficients are approximately proportional to the square of NIEL [Ref 3]. In the case of GaInP2/GaAs/Ge, the non-homogeneous design of the multi-junction does not lend itself easily to the NIEL concept. The results are inconclusive at present for relating the damage coefficients in GaInP2/GaAs/Ge to NIEL. However a recent work by D.C. Marvin of the Aerospace Corporation has revealed

relative damage coefficients for power, voltage, and current in GaInP2/GaAs/Ge triple junction solar cells. Table II-2 shows the ratio of the damage coefficient for 10 Mev protons to 1 Mev electrons. The values have accuracies up to 5% [Ref 4 pg. 1105]. These values will be used to equate the experimental data to 1 MeV equivalence. The 1 MeV equivalence can be calculated using equation 2.6.

$$\Phi_{(1MeV(e))} = C \times \Phi_{(10MeV(p))} \tag{2.6}$$

Where C is the relative damage coefficient, $\Phi_{(1MeV(e))}$ is 1 MeV equivalent fluence, $\Phi_{(10MeV(p))}$ is the fluence of the proton.

| Cell Type | Power | Voltage | Current |
|---|---|---|---|
| Spectrolab 2J | 492 | 759 | 412 |
| Spectrolab 2J EOL | 800 | 833 | 863 |
| TECSTAR 3J | 727 | 1235 | 489 |
| Spectrolab 3J | 612 | 824 | 414 |
| Spectrolab 3J EOL | 870 | 1020 | 565 |

**Table II-2. Equivalent Fluence Ratio for 1 Mev Electrons and 10 MeV Protons [From: Ref 4 pg 1105].**

THIS PAGE INTENTIONALLY LEFT BLANK

# III.  NPS LINEAR ACCELERATOR

## A.      INTRODUCTION

The Naval Postgraduate School electron linear accelerator (LINAC) was built in 1965.  It is similar in design and function to the MK III traveling wave LINAC at Stanford University.  In fact, the NPS LINAC was constructed of material used in a prototype accelerator from Stanford University.  The accelerator consists of three ten-foot sub-accelerator sections (that also functions as wave guides) each powered by a 22 Megawatts (peak power) klystron RF amplifier.  The RF pulse length is 3.5 microseconds and is cycled at 120 hertz.  Electrons can be accelerated up to 100 million electron volts (Mev) with an average electron current of 10 microamps. [Ref. 5: pg. 9&19].   A schematic of the NPS LINAC is found in Figure III-1.
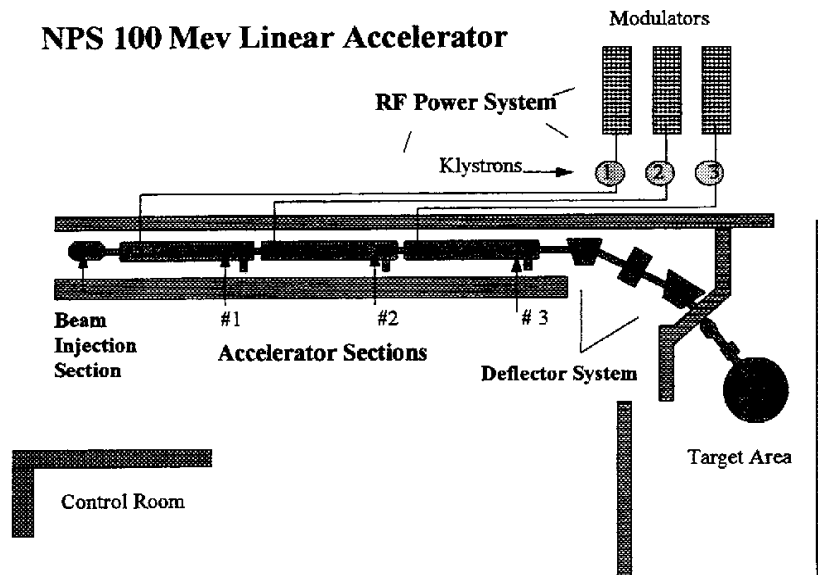


**Figure III-1.  NPS Linear Accelerator [From: Ref. 7: pg. 57].**

In this thesis the LINAC will be used to simulate the electron radiation environment that a multi-junction cell will experience in space.  So, the discussion of the LINAC will center on the theory and operation of the NPS LINAC that completes that objective.  Peripheral support systems will not be discussed.

## B. THEORY OF PARTICLE ACCELERATION

Charged particle (electrons and protons) motion is determined mainly by interaction with electromagnetic forces. The acceleration of charged particle is accomplished when kinetic energy is transferred to a particle by the application of an electric field. A particle will accelerate in the presence of an electric field as shown in Figure III-2. The voltage across the electrodes creates the electric field. So the acceleration is directly proportional to the voltage.
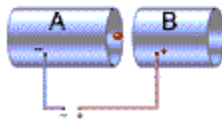


**Figure III-2. Basic Particle Acceleration [After: Ref 31].**

In order to properly simulate the radiation environment charged particles will have to be extremely energetic. Based on the ideas shown in Figure III-2 increasing the voltage across the electrodes should accelerate the electron to the desired velocity. This idea is not practical because at some point the air between the electrodes ionizes. Since we cannot keep increasing the voltage to get the electron up to the desired velocity, we must investigate an alternate solution. The solution is that we give the electron a sequence of smaller pushes with manageable voltages. One way to accomplish this is to use a linear accelerator (LINAC).

## C. THEORY OF ELECTRON LINEAR ACCELERATION

A LINAC is a type of particle accelerator in which charged particles are accelerated in a straight line. In a LINAC, the electrons pass through a series of electrodes. If the electrons are to keep accelerating, they must always be leaving a negative electrode and heading towards a positive one. Therefore the voltages on the electrodes have to be switched over as the electrons pass through. The switching has to be fast because the velocities of the electrons are approaching the speed of light. Figure III-3 shows basic linear acceleration.
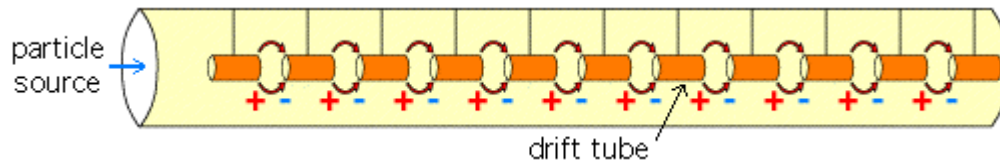
**Figure III-3. Schematic diagram of linear acceleration [From: Ref. 31].**

**D.     NAVAL POSTGRADUATE SCHOOL LINAC**

Now that we understand the basic theory of linear acceleration, the discussion will now center around the specifics of the Naval Postgraduate School LINAC.  The NPS LINAC is a traveling wave linear accelerator.  The basic theory of linear particle acceleration still applies, but an explanation is required to incorporate the traveling wave. This discussion will start with the electron beam injection and progress through the acceleration process and conclude with beam termination.

**1.     Electron Beam Injection.**

The 80 kev electron gun provides a well formed pulse of electrons with a short build up and decay period and a relatively constant amplitude during the pulse.  Electron injection occurs during each klystron pulse [Ref. 6].  This provides a group of electrons that have a predictable and uniform energy spectrum.  Electrons from the gun are traveling at about half the speed of light and the wave in the accelerator the speed of light.  With this speed differential, the binding of the electrons to the electromagnetic wave is difficult, and a number of electrons from the gun are lost.  This problem is solved by the use of a pre-buncher and drift space.  The pre-buncher serves to slow down the electrons that are too far ahead in phase and speed up those that are behind.   The drift space then allows the velocity differential to spatially bunch the electrons prior to entry into the first sub-acceleration section where they are bound to the RF wave [Ref 5]. Figure III-4 is a schematic of the Beam injection section
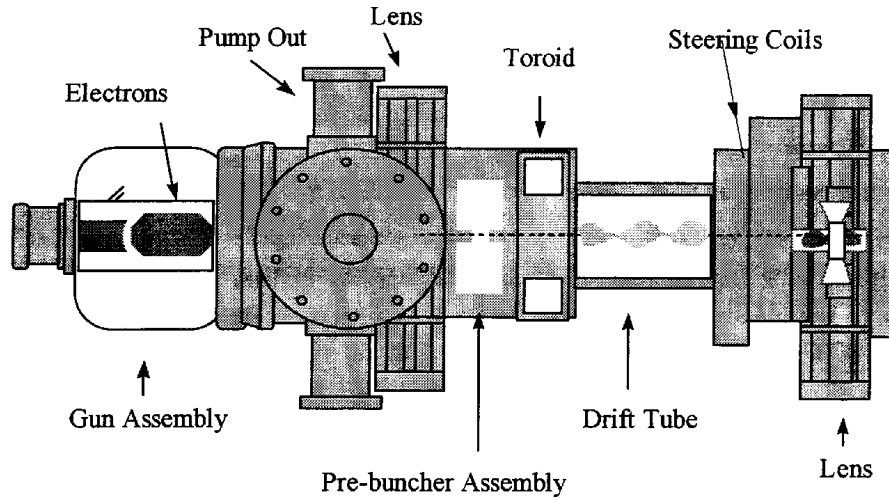
Figure III-4. Prebuncher Assembly [From: Ref. 7: pg. 68].

### 2. Sub-Acceleration Section.

Bunched electrons are accelerated in the copper structure of the accelerator section. The accelerator has three sub-acceleration sections. Figure III-5 is a schematic of one of the sections. However, the electrons will not experience acceleration unless the phase of the electromagnetic wave is correct. The electromagnetic wave that push the electrons in the LINAC are created by the microwaves from the klystrons in each of the three acceleration sections and are fed into the accelerator structure via the wave guides.

18
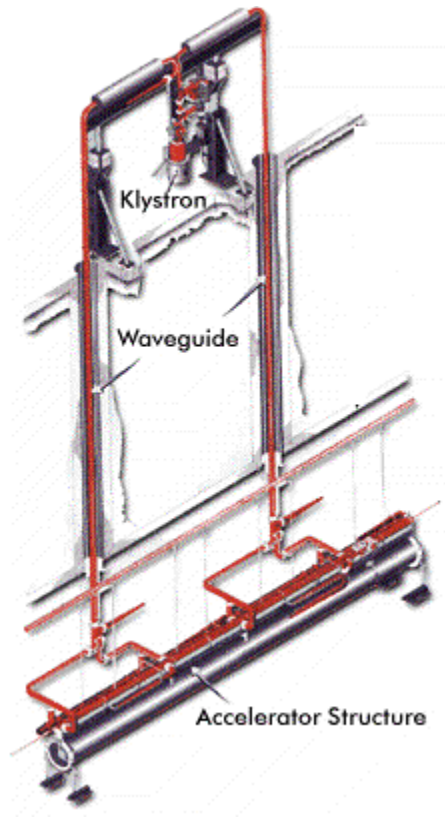
**Figure III-5. Accelerator section. Note: This is a schematic of an accelerator section from the MK III LINAC at Stanford. However, its functional design is identical to the NPS LINAC [From: Ref.6].**

The wave has two areas of phase that will affect the acceleration of the electron. These areas correspond to the rising side and the falling side of the wave (Figure III-6). The rising side is said to be unstable because any particle (on the rising side) behind the correct phase point will continually fall behind gaining too little energy for acceleration. By the same token any particle ahead of the correct phase point will be continually ahead and will have too much energy. The falling side of the wave is said to be stable because any electron ahead or behind the correct phase point will migrate back to the correct phase point. Thus a stable phase relationship. [Ref. 5: pg 11].
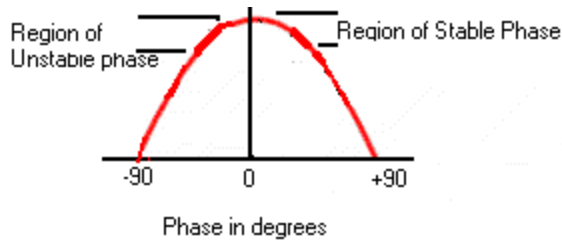
**Figure III-6.  Relative Phase of electrons.**

A common and simple analogy to describe this phenomenon is a surfer riding a wave (Figure III-7).  As long as the surfer stays on the crest of the wave he will continue to accelerate.  If he falls behind the crest he loses acceleration and eventually "wipes out."
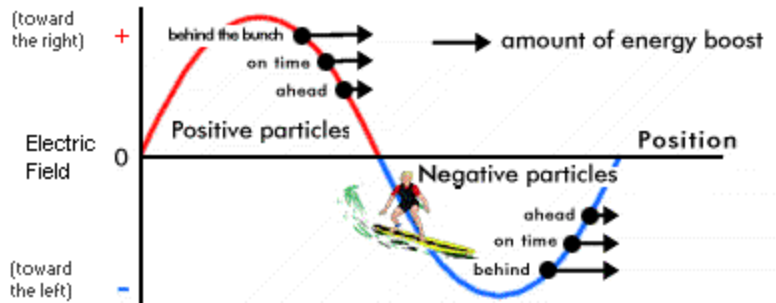


**Figure  III-7.   Surfer Analogy of Phase Stability [From: Ref. 6].**

### 3.      The Deflection System.

The final component of the accelerator is the deflection system shown in Figure III-8.  The accelerated electron beams exits the third sub-accelerator section and enters the collimator.  The collimator serves to produce an electron beam of low divergence. The first deflection magnet separates the various energies in the beam, so that the desired energy can be selected by the energy defining slits. This magnet also serves to deflect the electron beam so that the counting equipment is not in line with the undesirable forward radiation of the electrons.  The second magnet focuses the beam onto the target. [Ref. 5: pg 23].
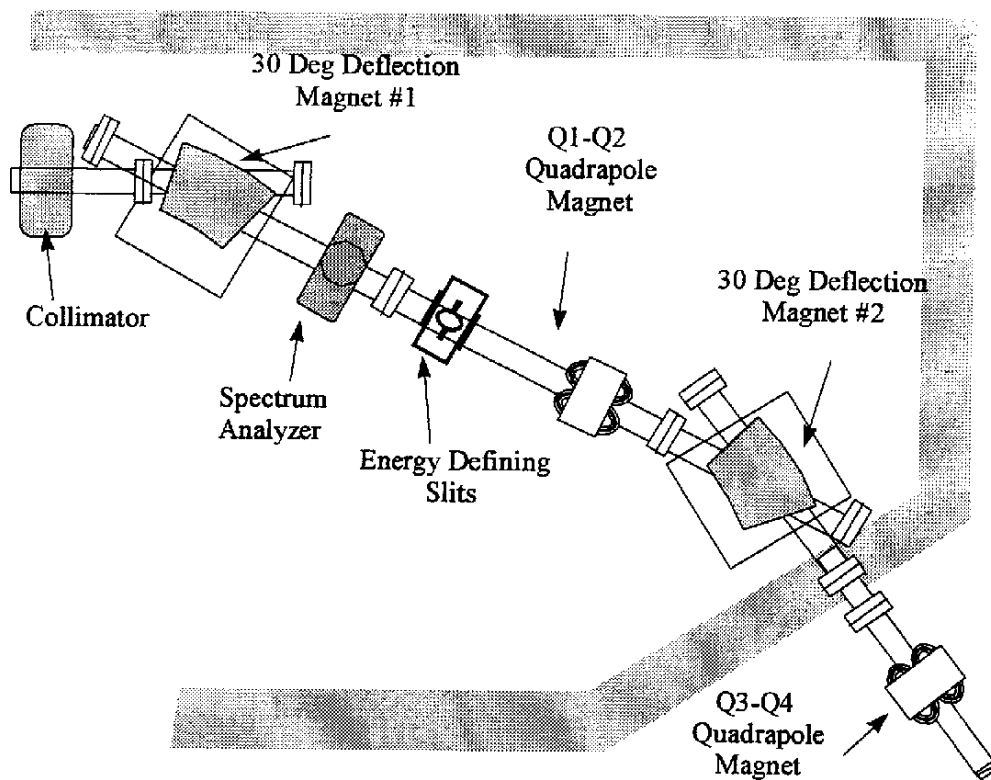
**Figure III-8. The Deflection System [From: Ref. 7: pg 75].**

### 4. The Target Chamber.

The electron beam terminates in the target chamber. The second deflection magnet focuses the beam onto the target. The target chamber is encased in concrete and cinder blocks to reduce radiation exposure. The target chamber just like the entire system is under vacuum. The system is under vacuum first to allow the transfer of energy to the beam to be as efficient as possible. Secondly, wherever the beam is intended to travel or high field gradients are present, there has to be a vacuum present to prevent the ionization of air. The ionized air would form a path to ground that would reduce the electric field.

Observation and control of the experiment was accomplished using video cameras and DC motors to control the target station. A phosphorous screen placed in front of the device under test assisted with imaging of the beam. The electron beam causes the screen to become florescent, and the video image is recorded. Imaging software and a personal computer creates a digital image.

The Secondary emission monitor (SEM), located at the back of the target chamber, was used to measure the fluence (#/area).  As the electron beam passes through the SEM, it causes a charge to accumulate on a capacitor. The capacitor is connected to digital voltage integrator in the control room. The total charge accumulated on the capacitor is determined by using the relationship.

$$Q = C \times V \tag{3.1}$$

Where Q represents the total charge, C is the value of the capacitor, and V is the measured voltage across the shunted capacitor. Since we know that

$$Q = n \times q \tag{3.2}$$

Where q is the charge per electron and n is the total number of electrons. Then the theoretical number of electrons that are passed through the SEM can be calculated as

$$n = \frac{C \times V}{q} \tag{3.3}$$

The SEM in the NPS LINAC is only 10% efficient.  Therefore, the total number of electrons can be expressed as:

$$n = \frac{C \times V}{q \times .1} \tag{3.4}$$

The beam fluence is usually represented as number of particles per unit area.  Thus we get the following relationship:

$$\Phi = n \div \frac{Beam}{Area} = \frac{C \times V}{q \times .1 \times A} \tag{3.5}$$

# IV.  SEMICONDUCTOR PHYSICS

## A.      INTRODUCTION

The photovoltaic effect is the basic physical process through which semiconductor material converts sunlight into electricity. In order to completely understand this phenomenon we must first examine a few principles of semiconductor physics.  Some of these principles will be illustrated using silicon, a Group IV elemental semiconductor.

## B.      CRYSTAL STRUCTURE

A semiconductor is made up of a lattice of atoms linked together through covalent bonding.  A silicon atom has 14 electrons in three different shells.  The inner two shells are full, but the outer shell (valence shell) is only half-full.  This outer shell contains only four electrons when it could hold as many as eight.  A silicon atom with four surrounding atoms will share each of its four outer electrons with each of the four neighbors to complete the valence shell.  This sharing of electrons is called covalent bonding.  Each silicon atom in the lattice has its own four outer electrons and one extra electron from four neighboring atoms, making a total of eight electrons. The lattice structure created from this arrangement is called the diamond lattice.  The diamond lattice or Zinc-blende structure is the typical lattice for most mass produced semiconductors.  The Zinc-blende crystal lattice structure results from Group III and V compounds that exhibit semiconductor properties.  Figure IV-1 illustrates both the diamond and Zince-blende lattice structure.

**Figure IV-1. Diamond and Zinc-blende Lattice Structures [From: Ref. 9 pg 10].**

A semiconductor is a material whose conductivity exists somewhere between that of electrical insulators and conductors.  The ability of a material to act like a semiconductor is based on the crystal structure. According to the quantum theory, the energy of an electron in the crystal must fall within well-defined states. These states vary from a ground state to an excited state.  The energies of valence electrons in the ground state are called the valence band. The excited stated is the conduction band.  The separation between the valence and conduction band is the energy gap or band-gap. Electrons cannot exist in the band-gap, also knows as the forbidden zone.

The width of the band-gap (Ec - Ev) is usually denoted by Eg (band-gap energy). Band-gap energy defines the minimum amount of energy required to free an electron from the outer valence of an atom. All materials based on their atomic structure have specific band-gap energies.   It has been determined experimentally that Eg depends on temperature (T).  The following expression shows that relationship [Ref 10 pg 6]:

$$E_g(T) = E_g(0) - \frac{\alpha T^2}{\beta + T} \tag{4.1}$$

Where $E_g(0)$, $\alpha$ and $\beta$ are the fitting parameters. Table IV-1 shows the fitting parameters that would be used to calculate the band-gap of selected material.

|  | Ge | Si | GaAs |
|---|---|---|---|
| $E_g(0)$ (eV) | 0.7437 | 1.166 | 1.519 |
| $\alpha$ (meV/K) | 0.477 | 0.473 | 0.541 |
| $\beta$(K) | 235 | 636 | 204 |

**Table IV-1. Parameters used to calculate the band-gap energyof germanium, silicon and gallium arsenide (GaAs) as a function of temperature [After: Ref. 10].**

It must be noted that semiconductor crystal structures have extremely complex energy bands and are not fully described in this thesis. The simplified band diagram of Figure IV-2 was sufficient for this thesis.
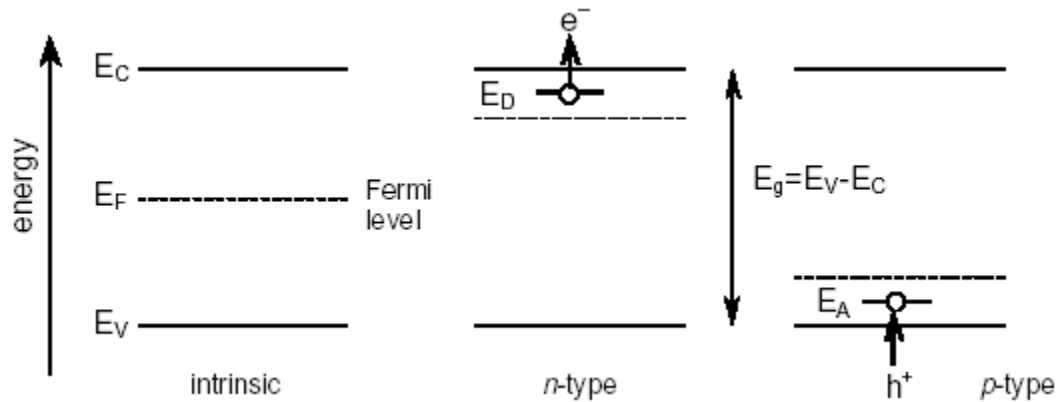


**Figure IV-2.  Energy diagram of semiconductors with intrinsic, n-type and p-type properties [From: Ref. 14: pg 10]**

## C.    CONDUCTION

Conduction in a semiconductor occurs when an electron transitions from the valence band to the conduction band.  And from the discussion above, it is clear that conduction in a semiconductor is temperature dependent.  In order for electrons to cross the energy gap, they must acquire sufficient energy, energy greater than the band-gap energy.  When the electron is elevated to the conduction band it leaves a hole.  A hole is positive charge carrier. Thus we have electron-hole pair generation. The electron and holes are the charge carriers and current flow is a result of their motion.

It is now important to distinguish between the two cases of intrinsic (pure) and extrinsic (doped) semiconductors.  In a pure semiconductor at T = 0 K (Kelvin), all states in the valence band are occupied, and there are no electrons in the conduction band. As the temperature is increased some electrons are excited into the conduction band. Each electron excited into the conduction band leaves behind a hole in the valence band.  Since the material is pure there are no excess charge carriers.  So, there are equal numbers of

electrons and holes in the material. Since there are no excess charge carriers, there is no motion of the electron hole-pairs generated. Therefore, there is no resulting current.

Extrinsic semiconductors are pure materials doped with impurities. Donor impurities add electrons, and since electrons are the majority carriers, the material is called n-type. Donor impurities have levels close to the conduction band and donate electrons to that band. Acceptor impurities accept electrons so that additional holes are formed. Positively charged holes are the majority carriers, so the material is p-type. The localized impurity levels are close in energy to the valence band. Since the acceptor levels are close to the valence band, the majority of those levels are occupied by holes. Figure IV-2 shows a band diagram for a n and p-type semiconductor.

Extrinsic (doped) semiconductors are important to solar cells because they have an increased number of positive and negative charge carriers. Increased carrier concentration, in general, increases the current capability of the solar cell. Also, the extra loosely bound electrons are advantageous because they are freed more easily. They are free to stimulate and perpetuate the formation of electron-hole pairs.

## D.    THE P-N JUNCTION

The operation of solar cells is based on the formation of a p-n junction. The p-n junction is formed by an interface of p-type and n-type semiconductor materials. At the junction, the electrons diffuse across the junction into the p-type region where hardly any electrons are present. Simultaneously, holes diffuse across the junction into the n-type region. The electrons that are diffusing from n to p leave behind uncompensated donor ions ($N_d^+$) in the n material, and holes leaving the p region leave behind uncompensated acceptors ($N_a^-$). The diffusion of electrons and holes continue until the p-region displays a negative charge and the n-region displays a positive. At this equilibrium state, there exist a built in electric field which is caused by the fermi energy difference between the n-type and p-type semiconductors [Ref. 9 pg 46]. The electric field will act as a potential barrier and give the p-n junction diode its principal characteristic, rectification. The p-n

junction will only permit significant conduction in one direction.  A significantly large voltage would have to be applied in order to overcome the repulsion of charges.

The region deplete of mobile charge carriers is known as the depletion region. The region contains the ionized acceptors and donors at the edges of the n-type and p-type regions respectively.  The depletion width (W) can be determined with the following expression [Ref 11 pg 146]:

$$W = \left[ \frac{2\varepsilon V_o}{q} \left( \frac{1}{N_a} + \frac{1}{N_d} \right) \right]^{\frac{1}{2}} \tag{4.2}$$

Where $\varepsilon$, q are constants and $N_a$, $N_d$ represent concentration of acceptors and donors.  $V_o$ is the potential difference that builds up between the n-type and p-type layers.  The width of the depletion region can be changed by applying an external voltage across the junction.  Figure IV-3 diagrams the p-n junction.
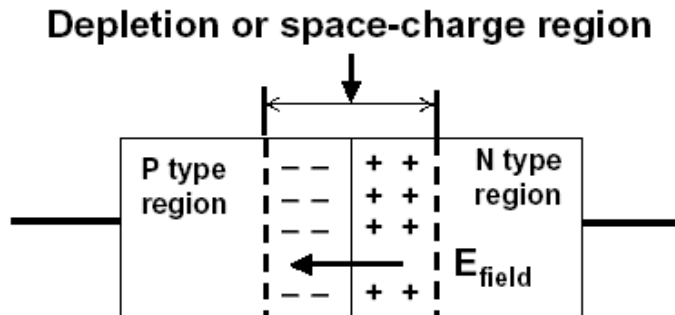


**Figure IV-3.  P-N junction and band diagram [After: Ref. 11 pg 143].**

## E.    SOLAR CELLS
### 1.    Photovoltaic (PV) Effect

Sunlight is composed of photons, or particles of solar energy. These photons contain various amounts of energy corresponding to the different wavelengths of the solar spectrum. When photons strike the material, they can be reflected, absorbed, or they may pass right through the cell. Only the absorbed photons, photons with energy (hv) greater

than the $E_g$ of the semiconductor, can be converted into electricity by the solar cell. The photon energy is described by equation 4.3. Table IV-2 lists the properties of some common solar cell semiconductor materials.

$$h \times \nu = h \times \left( \frac{c}{\lambda} \right) = \frac{1.24}{\lambda(\mu m)} \qquad (4.3)$$

Where h is Plank's constant, $\nu$ is the frequency of the photon, c is the speed of light, and $\lambda$ is photon's wavelength.

The absorbed photons promote electrons from the valence to the conduction band. Since holes are left behind in the valence band, the absorption process has generated electron-hole pairs. Electrons created by light in the p-type material migrate to the junction and are then swept across the p-n junction into the n-region. The holes created in n-type material are likewise swept into the p-region. The passage of these excess charge carriers, known as minority carriers (electrons in the p-region, holes in the n-region) creates a photocurrent and voltage difference at the solar cell terminals. Although there is a tendency for the electrons and holes to recombine, ideally most of them will only recombine when passing through an external circuit outside the material because of the internal potential energy barrier. Therefore, if a circuit is made, power can be produced from the cells under illumination, since the free electrons have to pass through the load to recombine with the positive holes.

The continuous generation of electron-hole pairs is the crux of conversion of light into electricity. So it should be apparent that the process is not a singular event. The incoming photons keep the process going by continually creating new electron-hole pairs. Figure IV-4 shows the PV process.
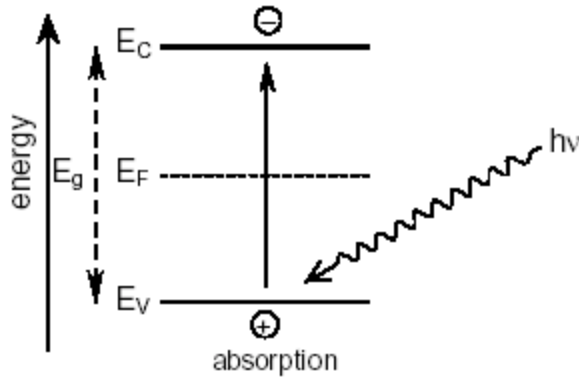
**Figure IV-4. Electron-Hole Creation from Light.**

### a. Recombination and Carrier Lifetime

The passage of minority carriers across the junction prevents electron-hole recombination. The minority carrier must be within a minority carrier diffusion length of the junction to be swept across the junction. The minority carrier diffusion length represents the average distance minority carriers can diffuse into a collection of majority carriers before recombination [Ref. 9: pg. 131]. Thus a photo-generated electron in p-region has a limited lifetime in the presence of the stable population of holes but an unlimited lifetime after crossing the junction into the n-type material. The lifetime ($\tau$) of the minority carrier is the average time an excess minority carrier will exist in the presence of majority carriers [Ref. 9: pg. 124]. The rate at which electrons and holes combine is given by the following equations:

$$\operatorname{Re} combination = \frac{\Delta p}{\tau} = \frac{\Delta n}{\tau} \tag{4.4}$$

Where $\tau$ is the carrier's life time, and $\Delta p$ and $\Delta n$ are the deviations in the carrier concentrations from their equilibrium values [Ref. 9: pg. 115].

| Material | Energy gap (eV) | Type of gap |
|---|---|---|
| crystalline Si | 1.12 | Indirect |
| Ge | 0.67 | Indirect |
| amorphous Si | 1.75 | Direct |
| CuInSe$_2$ | 1.05 | Direct |
| CdTe | 1.45 | Direct |
| YP | 1.00 | Direct |
| GaAs | 1.43 | Direct |
| Ga0.69Al0.31As | 1.66 | Direct |
| In0.496Ga0.504P | 1.93 | Direct |
| In0.5Al0.5P | 2.30 | Direct |
| ZnSe | 2.58 | Direct |

**Table IV-2.  Properties of Several Semiconductors [After: Ref. 12].**

## F.    SOLAR RADIATION

The air mass number determines the length of the path that the sunlight takes through the atmosphere.  As the length of that path increase the spectral irradiance decrease.   The spectrum of sunlight outside the earth's atmosphere spectrum is referred to as the Air Mass Zero (AM0) spectrum.  The AM0 spectrum closely fits the spectrum of a black body at 5800 K. The total power density is 1353 W/m$^2$ or 135.3 mW/cm$^2$ [Ref 7]. AM0 is the spectral irradiance solar cells experience in space.  So, the SS-1000 solar simulator must emulate the spectral irradiance of the sun.  The sun's spectral irradiance at various air masses is shown in Figure IV-5.
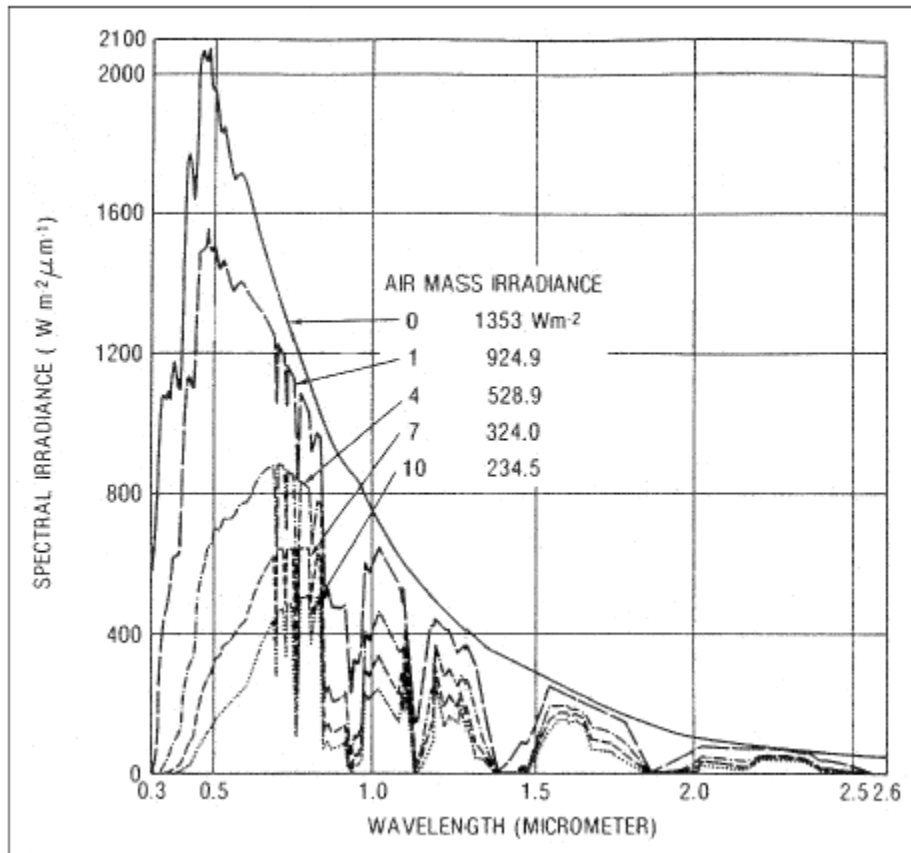
**Figure IV-5. Sun's Spectral Irradiance at Various Air Masses.**

## G. SPECTRAL RESPONSE

The spectral response of a photovoltaic device is a measure of the photo-generated current at a specific wavelength. The measurement of the wavelength dependence of the photocurrent is valuable not only as a characterization technique, but is essential for understanding current generation, recombination, and diffusion mechanisms in photovoltaic devices. Any change in the material properties or in the electronic structure of the device that affects these mechanisms will be reflected in the spectral response curve. The spectral response gives insight to how efficient incident photons generate electron-hole pairs in a semiconductor and a subsequent measurement can quantify degradation affects. Figure IV-6 is the external quantum efficiency measurement of a GaInP/GaAs/Ge multi-junction solar cell as reported by the National Renewable Energy Laboratory (NREL).
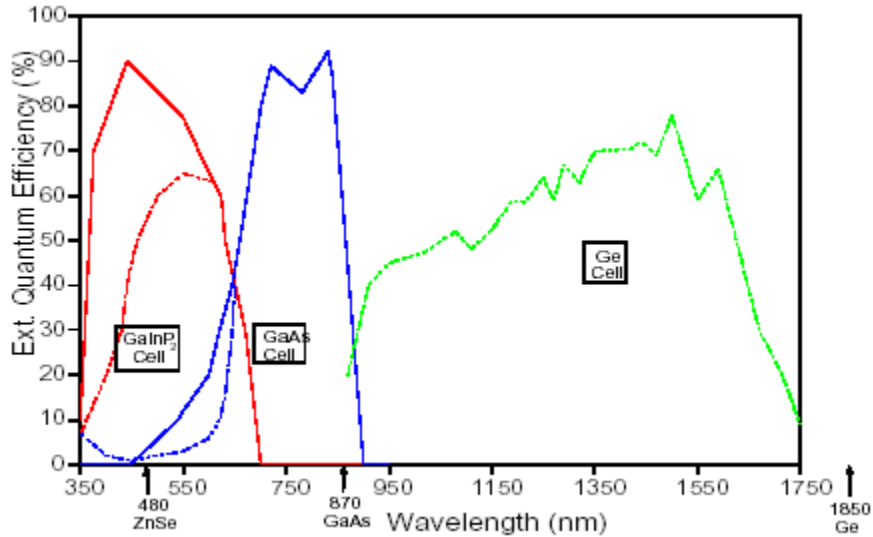
**Figure IV-6. External QE of a GaInP/GaAs/Ge tandem solar Cell. The dotted line: 1995 results; The real line: 1996 results [From: Ref. 15:pg 3]**

### 1. Spectral Response Measurement

In a spectral response (SR) measurement, the generated current, as a function of irradiated power and wavelength is measured. The spectral response of a solar cell can be used to calculate the quantum efficiency ($\eta_q$). The $\eta_q$ is the number of generated electrons per number of incident photons, as a function of wavelength [Ref. 13: pg 5]:

$$\eta_{q=} \frac{I_{ph}}{\varphi_0} \text{ where } \varphi_0 = \frac{I_0}{h\nu} \tag{4.5}$$

where $I_{ph}$ is the magnitude of the photocurrent produced, $\bullet_0$ is the incoming photon flux density, $I_0$ is the incident light density per unit area, $h$ is Planck's constant and $\bullet$ is the frequency of the incoming photons.

Due to equipment limitation the spectral response was not determined experimentally. The concept is included to ensure a complete understanding of the tools used to characterize and analyze solar cells. The measured spectral response can be used to calculate the $I_{SC}$ as shown in chapter two. Hence can be used to assess induced degradation. Figure IV-7 shows a schematic of a spectral response measuring system using light biasing. References 17 and 25 provide a more in depth explanation of spectral response measurement for multi-junction solar cells.

## Filter Spectral Response System 290-2000 nm
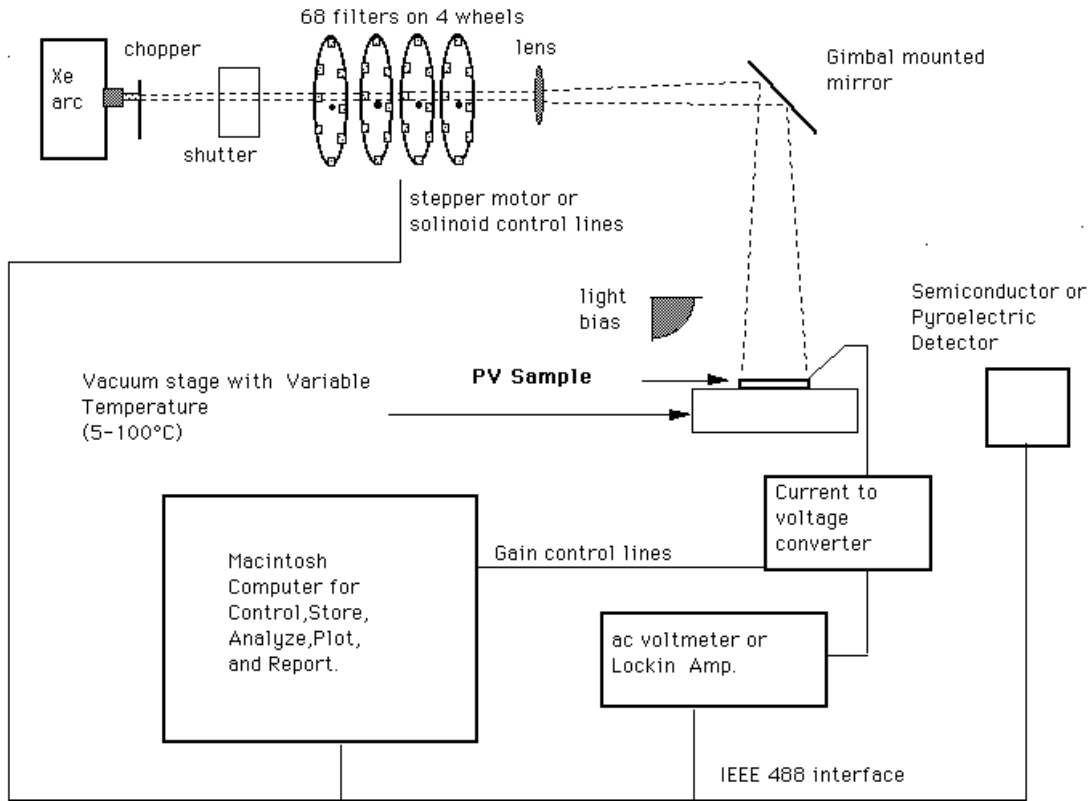


**Figure IV-7. Setup for Measuring the Spectral Response of a Solar Cell [From: Ref 17].**

## H.    SOLAR CELL PARAMETERS

Solar cells are characterized by quantities extracted from the cells' current-voltage (IV) curve.   A typical current-voltage curve is shown in Figure IV-8. The important operational parameters of the solar cells:

1.  Open circuit voltage ($V_{OC}$) is the threshold up to which the junction will power an electrical load and so convert light into electricity.

2.  Short circuit current ($I_{SC}$) is the current value at zero bias.

3.  Maximum current and voltage ($I_{mp}$, $V_{mp}$) are the values for I and V when most power is delivered:

$$P_M = I_{mp} \times V_{mp}$$                                                    (4.5)

33
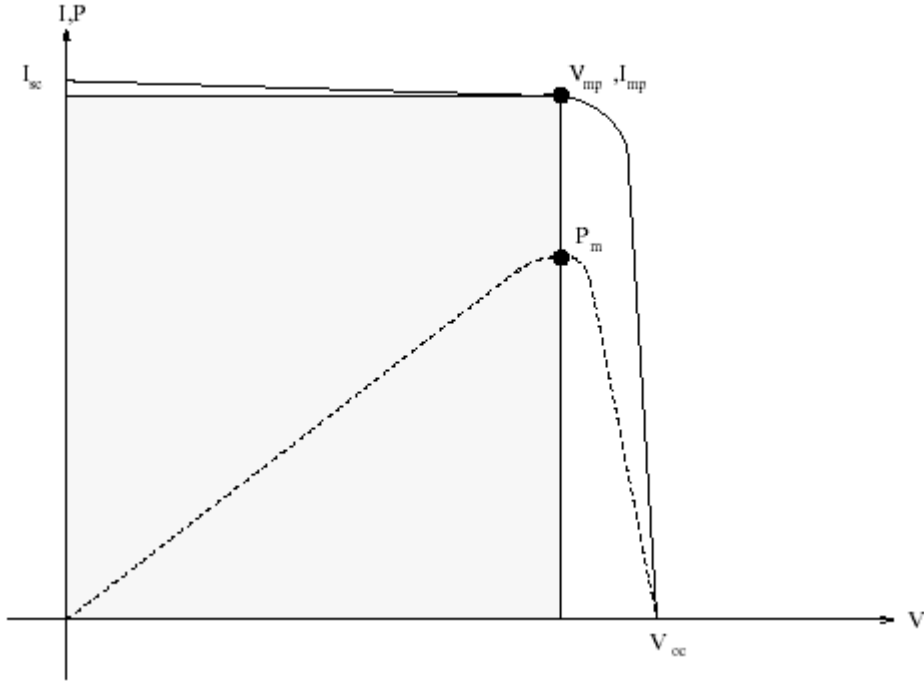
**Figure IV-8.  IV Curve and Electrical Parameters.**

4.  The fill factor (FF) is a measure how square the I-V curve is and hence how efficient the power extraction can be. The fill factor is defined as:

$$FF = \left( \frac{P_M}{V_{OC} \times I_{SC}} \right) \times 100 \qquad (4.6)$$

5.  The figure of merit for solar cell performance is the conversion efficiency ($\eta$), defined as:

$$\eta = \left( \frac{P_{OUT}}{P_{IN}} \right) x100 \qquad (4.7)$$

$$\eta = \left( \frac{P_M}{135.3 \times A} \right) \qquad (4.8)$$

Where 135.3 mW/cm$^2$ is the solar constant at AM0 and A is the surface area of the cell in cm$^2$.

# V.  MULTIJUNCTION SOLAR CELLS

## A.    INTRODUCTION

The light from the sun is made up of a range of wavelengths and corresponding photon energies.  The efficiency of single junction cells is partially limited by the inability to fully utilize the multiple photon energies in the incident wave.  Since electrons in the cell's material need a specific energy to overcome the band gap, an incident photon must have that same specific energy to free the electron from its binding. Photons with energies greater than the band gap, the fraction of energy greater than the band gap is lost as heat.  Photons with energies less than the band-gap pass through the material without generating electric power.

Once single-junction devices have been optimized for materials composition and quality and best device structure and processing, there are essentially two ways that solar cell efficiency can be substantially increased. One approach is to use concentrator solar cells.  Concentrator solar cells uses lens or mirror to concentrate the intensity of the sunlight striking the cell. The concentrated sunlight has the affect of increasing the open circuit voltage ($V_{OC}$), short circuit current ($I_{SC}$) and the fill factor (FF) thus the efficiency [Ref. 18: pg 933].

The next approach was to develop multi-junction solar cells that can utilize the total solar spectrum with different wavelengths. Solar cells are stacked with respect to the energy gap of the semiconductor. Multi-junction cells are also called tandem cells.

There are two types of multi-junction cells:  a mechanically stacked tandem cell and a monolithic tandem cell.  A mechanically stacked tandem consists of individually grown cells that are stacked and connected by transparent glue Figure V-1.  A monolithic tandem cell consists of multiple cells in which all cells are grown on top of each other in one growth-run connected by tunnel junctions.  Monolithic two-terminal tandems are the preferred design because of ease in compatibility in current systems both power generation and manufacturing.  The cells under study in this thesis are monolithic tandem cells.
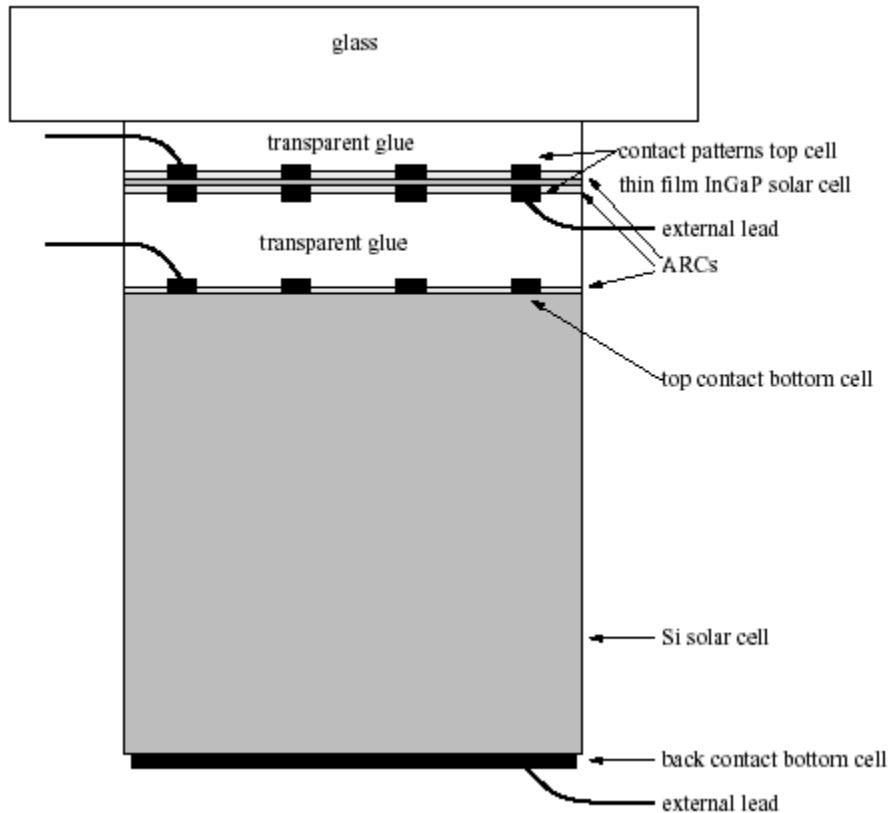
**Figure V-1. Mechanically Stacked Tandem Cell [After: Ref. 18].**

The multi-junction cell has more than one p-n junction, and different semiconductor materials are used to absorb different wavelengths of light. The cells are stacked with respect to the energy gap of the semiconductor as shown in Figure V-2. Large energy gap cells are located on the top of the multi-junction cell and smaller energy gap cells are built toward the bottom. The first layer of solar cells absorbs the high frequency light and allows the lower frequency light to pass through to the bottom solar cells. In order to fully understand the monolithic multi-junction cell we must expand the discussion of the p-n junction to include the tunnel junction.

AM0 Solar Spectrum (1350 W/m²)

$V_1$ — TOP CELL
$V_2$ — MIDDLE CELL
$V_3$ — BOTTOM CELL

$V_{photo} = V_1 + V_2 + V_3$
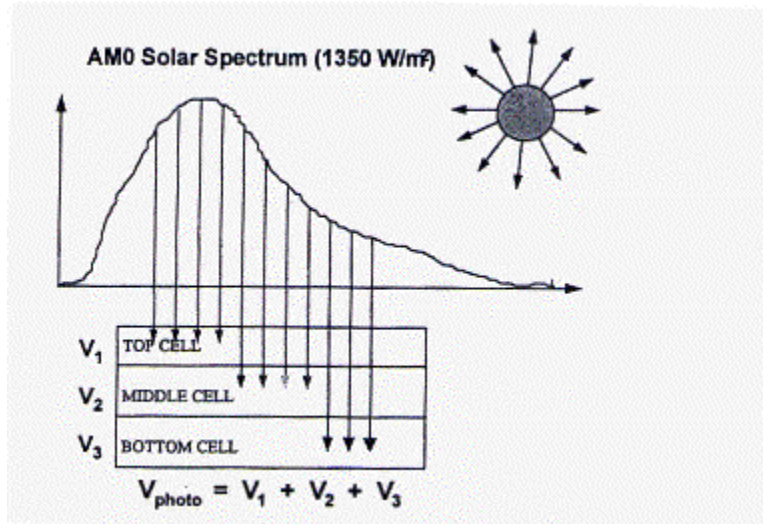
**Figure V-2.** **A multi-junction device is a stack of individual single-junction cells in descending order of band gap (Eg). The top cell captures the high-energy photons and passes the rest of the photons on to be absorbed by lower-band-gap cells [From: Ref. 15].**

### B. TUNNEL JUNCTION

The purpose of tunnel junction diodes is to monolithically interconnect cells of different band-gaps in series. So, the voltages of the cells are additive and the current is constant. The tunnel junction is a highly doped (in both the p and n region) p-n junction. The current-voltage characteristics (Figure V-3) of the junction show a peak and a valley in the forward direction due to the appearance of a negative resistance region (between points A and B) based on quantum tunneling [Ref. 19].
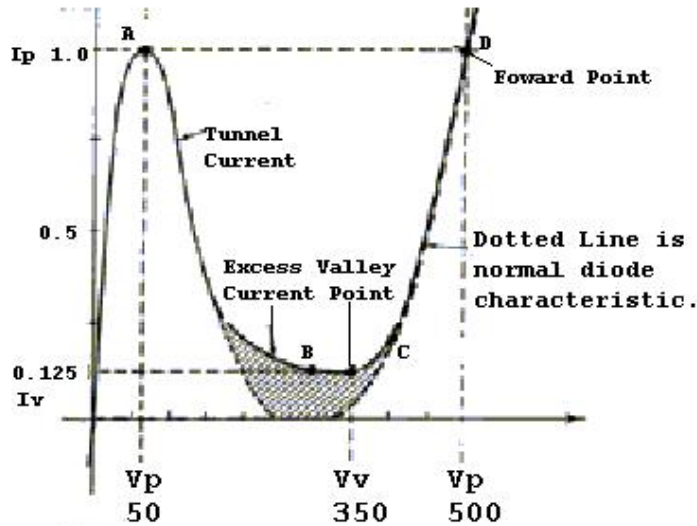
**Figure V-3. The current and voltage characteristics of a tunnel junction [From: Ref. 19].**

Quantum tunneling is the process by which a particle tunnels through a potential barrier (forbidden zone) to the other side. This phenomenon, as the name suggest, is only possible in quantum physic and not applicable in classical physics. However, according to classical physics, the particle's energy remains constant and neither the particle nor the potential barrier is damaged [Ref. 9: pg. 268-269]. Quantum tunneling is possible because the very high impurity density creates a junction depletion region so narrow that both holes and electrons can transfer across the p-n junction (Figure V-4).
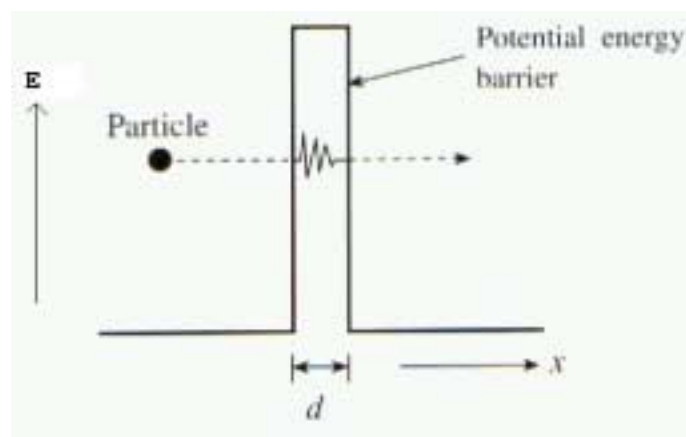


**Figure V-4. General Visualization of tunneling [From: Ref. 9: pg 269].**

38

The requirement for high efficiency in a multi-junction solar cell dictates that tunnel junctions have minimum electrical and optical parasitic losses. To this end, the resistance of the tunnel junction must be small so as not to increase the overall series resistance of the device. Next, the current density at the valley (Jv) must be higher than short-circuit current density (Jsc) of the multi-junction solar cell. This criterion ensures that the I-V curve for tunnel junction does not appear in the IV curve for the overall solar cell, thus reducing the fill factor [Ref. 20: pg. 1185].

In order to prevent optical power losses the tunnel junction cannot be photoconductive. The junction must allow the photons required for the sub-cells to propagate through the tunnel without being absorbed. Thus materials with wide band gaps are ideal for tunnel junctions. The thickness of the junction is constructed as thin as possible to further reduce the absorption of incident light.

## C.    LIMITS TO ACHIEVING THEORETICAL EFFICIENCY

Multi-junction solar cells achieve the high conversion efficiency by stacking cells made of semiconductor material with different band-gaps. Theoretical analysis indicates that the optimum efficiencies for multi-junction solar cells can reach as much as 41% [Ref. 21]. Theoretical efficiencies for multi-junction solar cells are shown in Table V-1.

| Device | AM0<br><br>1 Sun | AM1.5<br><br>500 Suns |
|---|---|---|
| 2 Junction | 31% | 36% |
| 3 Junction (with Ge) | 35% | 42% |
| 3 Junction (with 1-eV) | 38% | 47% |
| 4 Junction | 41% | 52% |

**Table V-1.  Theoretical Efficiencies for Multi-Junction Solar Cells [From: Ref. 21].**

The state-of-the-art solar cell for space power is the monolithic GaInP2/GaAs/Ge multi-junction solar cell with an efficiency of 26.8%. If the optimum band-gaps could be

utilized, the production efficiency could approach theoretical values. Figure V-5 shows optimum band-gaps and resulting efficiencies.
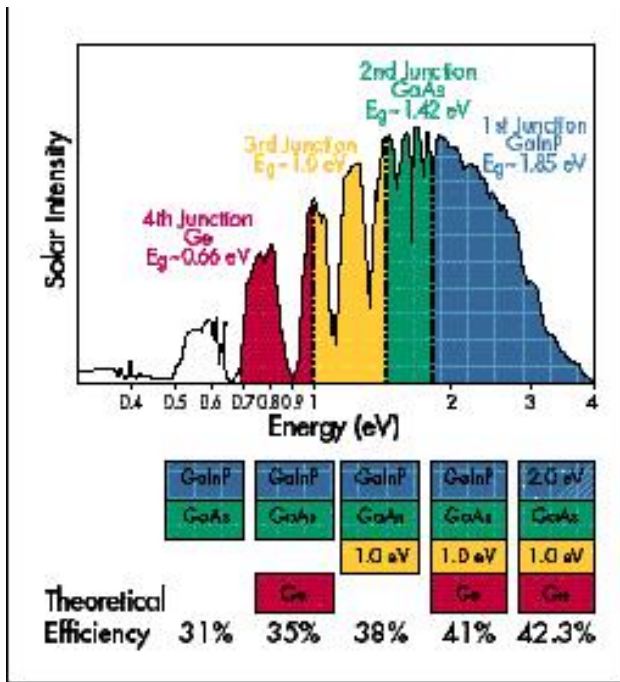


**Figure V-5. Theoretical Efficiencies and Optimum Band-gaps [From: Ref. 22].**

Unfortunately, no group of materials satisfies both the lattice-match and optimum band-gap requirements. Silicon and the III-V materials have crystalline structures and it is impossible to grow a robust structure of one crystalline material on top of another unless they have very similar lattice constants. The lattice constant defines the distance between the atoms in the structure. If the two crystalline materials lattice constants match within 2%, then very thin layers of one material can be grown on the other material. If, the match between lattice constants exceeds 2% or thick layers are grown, the strain between the material results in defects in the material [Ref. 23: pg 2]. Figure V-6 shows band-gap energy and lattice constants of various semiconductors at room temperature.
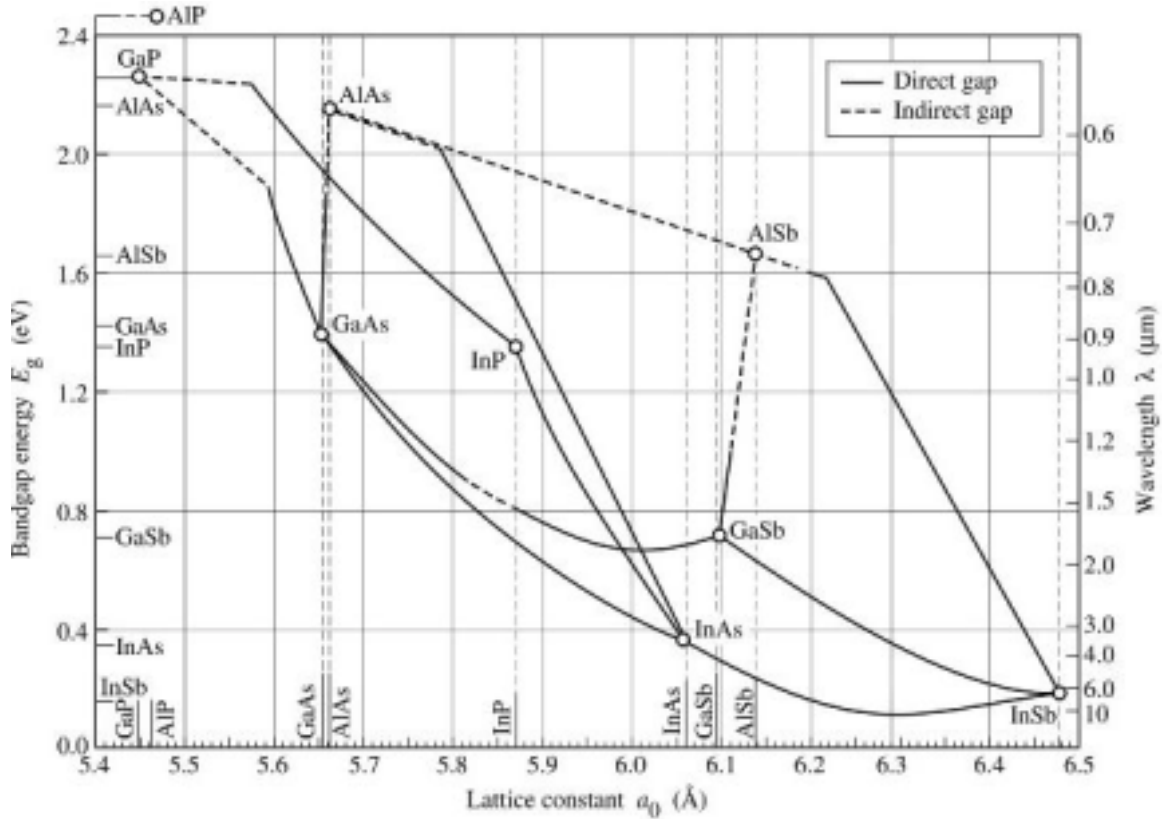
**Figure V-6. Band gaps and lattice constants semiconductor materials [From: Ref. 10].**

Another constraint related to the lattice match is the current matching between sub-cells. In a multi-junction solar cell, each junction generates current from a specific wavelength of the incident light. The current depends on the spectral response and thickness of each junction. Table V-2 shows the maximum achievable short circuit current for each sub-cell of an InGaP/GaAs/Ge triple junction solar cell [Ref. 24: pg 1]. Since, the cells are connected in series, the current value must be the same for all cells. The cell thickness has to be adjusted to generate equal currents, since the total current equals the lowest generated individual current. Current mismatches will result in efficiency losses.

| Subcell | Maximum Achievable $J_{sc}$ (mA/cm$^2$) |
|---|---|
| 1.86 eV InGaP | 22.1 |
| 1.42 eV GaAs | 15.6 |
| 0.66 eV Ge | 42.4 |

**Table V-2. Maximum achievable $J_{SC}$ for each subcell in an InGaP/GaAs/Ge triple junction Solar Cell [From: Ref. 24: pg 1].**

# VI. EXPERIMENT

## A. INTRODUCTION

The investigation and interpretation of the damage mechanism from electron irradiation in Spectrolab's GaInP$_2$/GaAs/Ge triple junction cell is the purpose of this thesis. Electrical characteristics were measured before and after irradiation to determine degradation of electrical parameters. This chapter will provide a description of the test cell, equipment, test procedure and test plan.

## B. GAINP2/GAAS/GE TRIPLE-JUNCTION SOLAR CELL

The state-of-the-art solar cell for space power is the monolithic GaInP$_2$/GaAs/Ge multi-junction solar cell. The cell's lattice matched material, high efficiency, and radiation hardness makes it ideal for space application. The material composition was chosen for their lattice constant match rather than their optimum ability to convert the solar spectrum. Table VI-1 shows the lattice properties and energy band gaps of the solar cell's material. The Ge sub-cell is not the optimal bottom cell as discussed in chapter V. A sub-cell of approximately 1ev would be ideal to efficiently convert the solar spectrum. Currently, there is not a lattice-matched material with a band gap of 1ev. The n-on-p design enhances the radiation hardness of the solar cell because with an n-on-p design the minority carrier diffusion lengths are longer after irradiation. Specifically, a multi-junction cell with a BOL efficiency of approximately 26% when radiated with 1x $10^{15}$ e/cm² 1 MeV equivalence, results in an EOL efficiency of 21%.
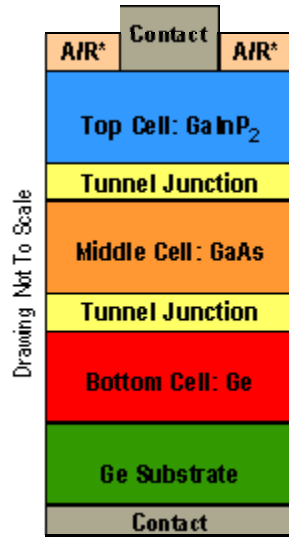
**Figure VI-1. Spectrolab GaInP2/GaAs/Ge Triple-Junction Solar Cell [From: Appendix A].**

| Material | Lattice Type | Lattice Constant (Å) | $E_G$ (eV) |
|---|---|---|---|
| GaInP$_2$ | Zinc Blende | 5.65 | 1.86 |
| GaAs | Zinc Blende | 5.65 | 1.42 |
| Ge | Zinc Blende | 5.66 | .6 |

**Table VI-1.  Lattice Properties of Solar Cell Material.**

## C.    SPECTRAL CORRECTION

Analysis of current-voltage (IV) characteristics is one of the most important diagnostic measurements used to characterize solar cells. In order to get accurate measurements under simulated conditions, the spectral irradiance of the simulator must be accurately represented.  The most common technique to ensure the proper spectral irradiance, involves a calibrated reference cell and spectral mismatch factors between the test and reference cell and the source and reference spectrum.  If the spectral response of the reference cell matches that of the test cell, accurate IV measurements can be made with the SS 1000 simulator.  However, if a spectral a mismatch exists between the reference cell and the test cell (i.e., reference cell is silicon and the test cell is GaAs), an error is induced which is proportional to the deviation of simulator's spectral irradiance from the standard solar irradiance.  The spectral mismatch factor **M** is given by [Ref. 27: pg 1097]:

$$M = \frac{\int E_r(\lambda)\,SR_r(\lambda)\,\partial\lambda}{\int E_c(\lambda)\,SR_r(\lambda)\,\partial\lambda} * \frac{\int E_c(\lambda)\,SR_{tst}(\lambda)\,\partial\lambda}{\int E_r(\lambda)\,SR_{tst}(\lambda)\,\partial\lambda} \qquad (6.1)$$

Where:

$SR_r(\lambda)$ = Measured spectral response of reference cell (A/W)

$SR_{tst}(\lambda)$ = Measured spectral response of test cell (A/W)

$E_c(\lambda)$ = Measured spectral irradiance of calibration spectrum ($Wm^{-2}nm^{-1}$)

$E_r(\lambda)$ = known spectral irradiance of reference spectrum ($Wm^{-2}nm^{-1}$)

When a spectrum mismatch exists the simulator's intensity is adjusted according to the following:

$$I_{rr} = \frac{I_{rc}}{M} \qquad (6.2)$$

Where:

$I_{rr}$ = Reference cell corrected Isc for desired (reference) spectrum (A)

$I_{rc}$ = Measured Isc of reference cell for calibration spectrum (A)

However because of the non-linear nature of multi-junction solar cell, current voltage measurements under AM0 conditions cannot be calculated directly from measurements under non-AM0 conditions using spectral-correction methods [Ref. 28: pg 158]. Therefore the most direct method to ensure accuracy of measurements is to match the simulator's irradiance as close as possible to AM0 conditions through design and adjustment. Furthermore, the reference cell should match the spectral response of the test cell.

Reference cells are radiometers used for measuring illumination levels when characterizing solar cells. By quantifying the amount of light reaching a test device, they enable the light-to-electricity conversion performance of solar cells to be measured and compared. A reference cell's calibration specifies the magnitude of the electrical signal it produces when the cell is illuminated with light of a particular spectral and total

irradiance.  The data for the reference cell under AM0 condition is shown in Table VI-2. The current an power values were divided by the area in the experimental procedures  to get current and power densities.

| Parameters | Value (units) |
|---|---|
| $V_{oc}$ | 2.517 [V] |
| $I_{sc}$ | 62.1 [mA] |
| Efficiency | 23.84 |
| $P_M$ | 129 [mW] |
| Fill Factor(FF) | 82.53 |
| $V_M$ | 2.193 |
| $V_M$ | 59 [mA] |

**Table  VI-2. Calibration Cell Photovoltaic Parameters [From: Appendix A].**

**D.      SOLAR SIMULATOR**

The simulator used in this research was an Optical Radiation Corporation model SS-1000.   The SS-1000 uses a xenon bulb that closely approximates the spectral distribution of sun light under AM0 conditions as shown in Figure VI-2.   The entire simulation and test set-up consists of the SS-1000, a Hewlett-Packard programmable power supply (HP 6626A), vacuum assisted/ temperature controlled brass test block, and a personal computer with an HP-IB interface card running LABVIEW software. Figure VI-3 shows the experimental set-up.
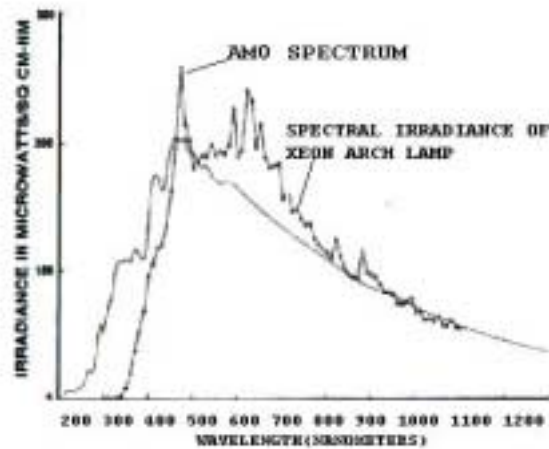
**Figure VI-2. Xeon Arch Lamp and the Sun's Spectrum at AM0 Conditions [From: Ref 1: pg 2-5].**
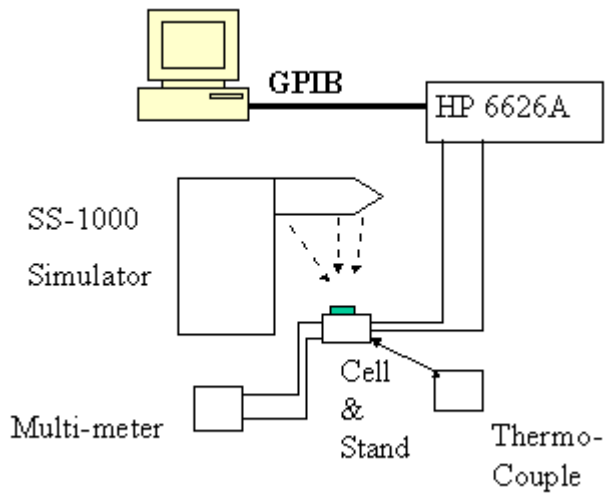


**Figure VI-3. Solar Simulation Set-up**

## E.    SOLAR SIMULATION SYSTEM

The SS-1000 illuminates the cell under test.  Since $V_M$, $I_M$, and $I_{SC}$ all vary as a function of temperature, the cell was mounted on a water-cooled brass block, cooled by a constant temperature water re-circulator.  The vacuum pump attached to the test block

ensures that the cell maintains proper thermal and electrical contact. A digital multi-meter is connected directly to the test block to monitor $V_{oc}$ or $I_{sc}$ of the cell under test.

The HP 6626A programmable power supply was used to both sink and source current to the cell under test. During cell illumination, the generated current is sunk into the power supply. The power supply also provides a variable voltage for $V_{oc}$ and a four volts bias to the test cell's voltage output. The bias voltage is needed because the HP 6626A cannot measure below four volts. The 4 volts must be subtracted from the measured voltage when processing data. Figure 3 shows the wiring diagram of the test cell and HP 6626A programmable power supply.

A Pentium based personal computer (PC) provided experiment control using the LabView™ Version 5.0 software. LabView™ is a virtual instrumentation program that allows precise control of the represented test instrument. The instrument represented and controlled was the programmable power supply. The computer was connected to the programmable power supply via an IEEE-488 General Purpose Interface Bus (GPIB) [Ref 3, pg. 5]. During cell illumination, LabView™ increments the power-supply voltage from zero volts to the point where the load creates a virtual open circuit, $V_{oc}$. Note: the point at zero volts corresponds to the short circuit current ($I_{sc}$). The voltage was incremented in .005 volts steps. The test cell's output voltage and current were measured at each interval and stored in a data file. LabView™ also uses the data to plot and display an IV curve in the active window.

## F.    CALIBRATION PROCEDURE

Calibration of the SS-1000 was accomplished by mounting the reference cell onto the test block. The reference cell used was a GaInP2/GaAs/Ge cell manufactured by Spectrolab. The cell was chosen to match the spectral response of the cells being investigated in this thesis. The cell was then illuminated with a Xeon lamp in the SS-1000 simulator. The lamp's intensity was set by adjusting the three focus adjustments that control the X, Y, Z positioning of the lamp so that the short circuit current of a calibration cell was identical to that measured under AM0 conditions (TableVI-2). Fine intensity adjustments were made by adjusting the lamp voltage.
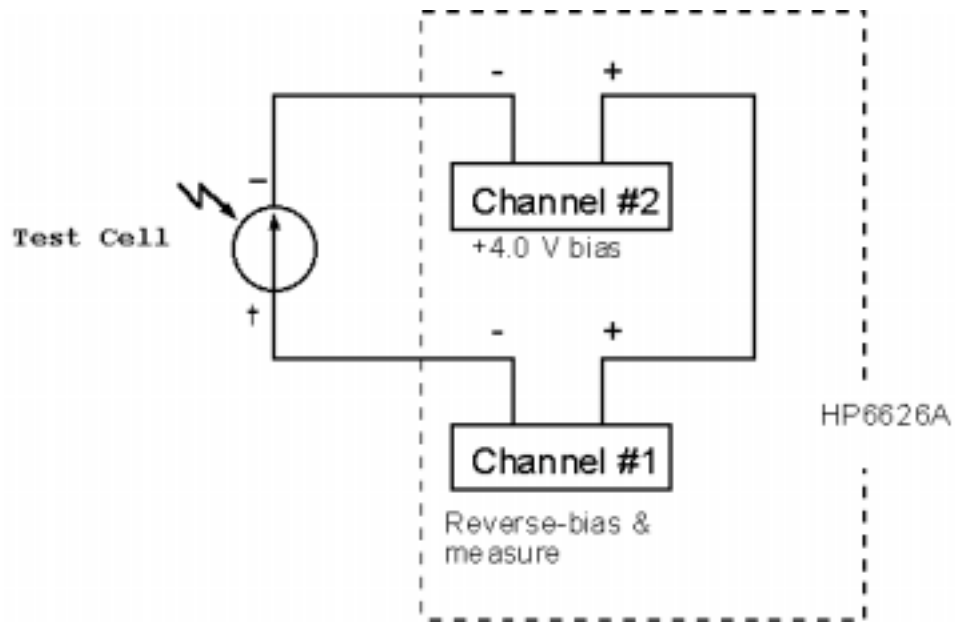
**Figure VI-4. Schematic of Test Cell and HP6626A [After: Ref. 29: pg 4].**


Once the simulator was adjusted to AM0 conditions with respect to the reference cell, an IV curve was generated for the reference cell and used for comparison. A calibration check will be run at the beginning and ending of a data set. A data set includes the beginning of life (BOL) test and the test after each stage of radiation.

## G. RADIATION PROCEDURES.

Accelerated electrons from the NPS LINAC will be used to irradiate Spectrolab's GaInP$_2$/GaAs/Ge triple-junction solar cells. The density profile of the electron beam in the LINAC is Gaussian. A digitized image of the electron beam is shown in Figure VI-5. The imaging of the beam was accomplished using video cameras and software installed in an IBM computer. Since the beam is Gaussian, the electron distribution can be determined. However, the digitized beam profile is the beam striking the phosphorous screen not the target. Thus the actual distribution of electrons per unit area is in question. The solution was to manipulate LINAC current, target distance and exposure time to get the Gaussian beam to essentially cover the target. An EXCEL program created by Professor Todd Weatherford was used to optimize these parameters to achieve a distribution of the beam in electrons/cm$^2$. The program calculates both beam distribution on the target and compares it to the phosphorus screen. Plots generated from the EXCEL

program demonstrating the electron beam distribution and target are shown in Figure VI-6.  The program called "Beam Profile" is included as Appendix B. The voltage equation 3.4 from the LINAC chapter was also used to calculate the exposure time required to accumulate the required fluence.

$$n = \frac{C \times V}{q \times .1}$$ (6.3)

Where C is the capacitance of the shunted capacitor and SEM($\eta$) was 10%.   This calculation serves as a comparison to the Beam profile program.

The standard dose for assessing electron damage to a solar cell is a fluence of $1 \times 10^{15}$ electrons/cm$^2$.  The resulting degradation to cell output power is appreciable.  The appreciable degradation allows for unambiguous comparison thresholds when comparing pre-irradiated data to irradiated data.

## H.    TEST PLAN

The electrical characteristics of the multi-junction cells were measured to establish their pre-irradiation electrical parameters. Table VI-3 shows the BOL parameters for the cells investigated in this thesis.  IV curves for the BOL are located in Appendix C.

The cells were to be irradiated with 90 Mev electrons and total fluence of $1 \times 10^{15}$ electrons/cm$^2$.  The electrical characteristics were to be measured at intervals of $1 \times 10^{14}$ electrons/cm$^2$ of irradiation. These characteristics were to be plotted as curves of electrical degradation vs fluence.  Due to the LINAC malfunctioning, the irradiation was not completed.   There was data for only one value of fluence at $5 \times 10^{14}$ electrons/cm$^2$. The irradiation data is presented in section VI-I.  The EOL IV curves resulting from the data is located in Appendix C.

| Cell # | Voc | Isc (mA/cm2) | Pm (mW/cm2) | FF | Eff (%) |
|---|---|---|---|---|---|
| MJ1 | 2.5843 | 15.16625025 | 32.85700116 | 83.83141 | 24.28455 |
| MJ2 | 2.5824 | 14.5962495 | 32.27815442 | 85.63354 | 23.85673 |
| MJ3 | 2.5814 | 14.8925 | 33.27353817 | 86.55179 | 24.59242 |
| MJ4 | 2.5748 | 14.77124975 | 32.89446825 | 86.48925 | 24.31225 |
| MJ6 | 2.5852 | 15.2749995 | 33.2726225 | 84.2581 | 24.59174 |

**Table VI-3.  BOL Parameters for Test Cells.**
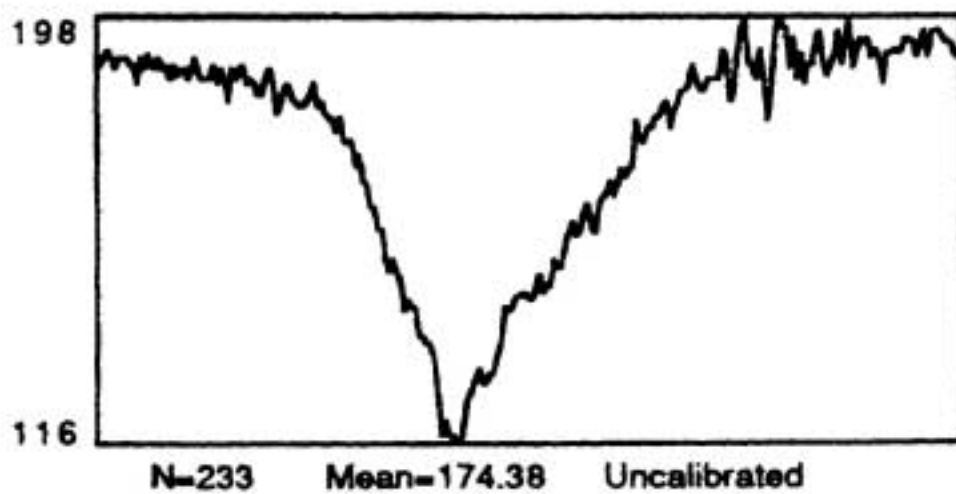
**Figure VI-5.  Density Profile Plot of the LINAC Electron Beam**
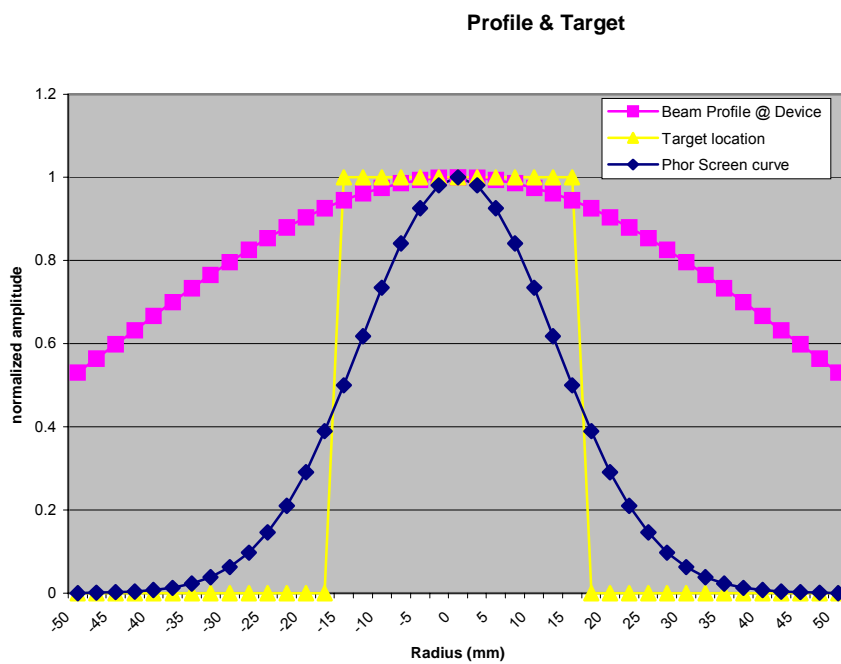


**Figure VI-6.  Gaussian Electron Beam Distribution and Target**

# I.    ELECTRON IRRADIATION TEST RESULTS

In this test we irradiated test cell #4.  The electron energy and fluenced used in this test were 90 MeV and 5x1014 e/cm2, respectively.  The IV results for the irradiated cells are summarized in Table VI-4.  The IV parameters with subscript 1, (ie.,VOC1), refers to BOL parameters.  IV parameters with subscript 2, refers to EOL parameters at a fluence of 5x1014 e/cm2.  As expected, ISC and VOC were degraded thus the efficiency ($\eta$).  Table VI-4 shows the ratios.  This type of degradation is representative of damage solar cells would experience when the cells transverse the outer Van Allen belt where the electrons energies are higher and more dynamic.  However, to make a conclusive determination concerning the degradation observed more data must be examined.

| $V_{OC1}$ (V) | $V_{OC2}$ (V) | Ratio | $I_{SC1}$ (mA/cm$^2$) | $I_{SC2}$ (mA/cm$^2$) | Ratio |
|---|---|---|---|---|---|
| 2.5748 | 2.4083 | .935 | 14.77124975 | 13.39375 | .906 |
|  |  |  |  |  |  |
| FF1 (%) | FF2 (%) | Ratio | $\eta1$ | $\eta2$ | Ratio |
| 86.48925 | 81.72 | .94 | 24.3 | 19.5 | .802 |

**Table VI-4.  IV Test Results for BOL and EOL.**

# VII.  CONCLUSION

Due to a malfunctioning electron gun, the NPS Linear Accelerator is not currently operational.  As a result, the radiation effects on the test cells could not be determined experimentally.   There was only one successful irradiation of cell number 4.  It was radiated with what was believed to be a fluence of $5x10^{14}$ e/cm$^2$.  The digitized beam profile, which is Gaussian, showed the distribution on the phosphorus screen not the target.  When the sigma of the beam was compared to the target area, the uniformity of the distribution was questioned as discussed in the experimental chapter.  The next intended step was to compare the $5x10^{14}$ e/cm$^2$ data to subsequent run using the Beam Profile program to determine if the degradation was comparable.  As mentioned earlier the irradiation could not be completed due to equipment failure.

Although the irradiation portion was not completed, there were some recommendations and observation worth noting.   The first recommendation is that the irradiation of the triple-junction cell be completed in subsequent thesis work.

Secondly the solar cell simulation/testing equipment should include the ability to accomplish quantum efficiency measurements.  As pointed out in chapters two and four, the quantum efficiency measurement is an effective tool for characterizing and evaluating solar cells.

The next recommendation is that the final results of this experiment and related thesis work be used to expand and improve the Silvaco model of the Multi-junction cell. Since the commercialization of this technology is relatively new, the Silvaco model is not yet complete.  Brenden P.  Lewis completed a Masters Thesis at NPS on the "Dark Current Analysis and Computer Simulation of Triple-Junction Solar Cells" in 1999.  This thesis did not include radiation effects.  A complete simulation of a space solar cell should include the ability to represent radiation effects. Future work in this area should include a range of electron energies to further improve the modeling accuracy of radiation effects.

Finally, the only observation made concerned annealing. It was observed that the cell number four experienced some annealing. The IV curve showing this effect is located in Appendix C. However, the question remains: was the annealing a result of a room temperature phenomenon or was it related to the current passed through the solar cell to affect the IV measurements? Subsequent work should investigate annealing.

# APPENDIX A.  MANUFACTURER'S DATA SHEET.

## Features

- High efficiency n/p design
  - BOL: up to 26% minimum average efficiency (28°C, AM0)
  - EOL: up to 21% minimum average efficiency (28°C, AM0, 1E15 e/cm² 1 MeV equivalence)
  - Integral bypass diode protection
  - Transparent insertion into existing systems

- High volume production capability:
  - Currently delivering 24.5% min. avg. efficiency solar cells
  - 26% minimum average efficiency available in year 2000
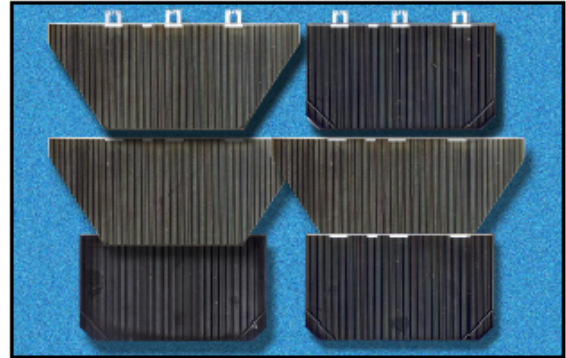


## Product Description

| | |
|---|---|
| Substrate | Germanium |
| Method of GaAs Growth | Metal Organic Vapor Phase Epitaxy |
| Device Design | Monolithic, two terminal triple junction. n/p GaInP$_2$, GaAs, and Ge solar cells interconnected with two tunnel junctions |
| Sizes | Up To 30 cm² |
| Assembly Method | Multiple techniques including soldering, welding, thermocompression, or ultrasonic wire bonding |
| Integral Diode | Si diode integrated into recess on back side |
| Note: Other Variations Are Available Upon Request | |

## Heritage

- More than 525 kW of multi-junction cells produced

- More than 85 kW of multi-junction arrays *on orbit*

- 1 MW annual capacity - cells, panels & arrays

- On orbit performance for multi-junction solar cells validated to ± 1.5% of ground test results

**S P E C T R O L A B**

A **BOEING** COMPANY

Spectrolab, Inc.
12500 Gladstone Avenue
Sylmar, California, USA  91342-5373
Ph: 1 (818) 365-4611  Fax: 1 (818) 361-5102

www.spectrolab.com

# S P E C T R O **D A T A**

## Typical Electrical Parameters
(AMO (135.3 mW/cm²) 28°C, Bare Cell)

$J_{sc}$ = 15.60 mA/cm²

$J_{mp}$ = 14.90 mA/cm²

$J_{load mn avg}$ = 14.93 mA/cm²

$V_{oc}$ = 2.545 V

$V_{mp}$ = 2.275 V

$V_{load}$ = 2.220 V

Cff= 0.85

$Eff_{load}$ = 24.5%

$Eff_{mp}$ = 25.1%

## Radiation Degradation
(Fluence 1MeV Electrons/cm²)

| Parameters | $1 \times 10^{14}$ | $3 \times 10^{14}$ | $1 \times 10^{15}$ |
|---|---|---|---|
| Imp/Imp₀ | 0.99 | 0.97 | 0.90 |
| Vmp/Vmp₀ | 0.97 | 0.95 | 0.92 |
| Pmp/Pmp₀ | 0.96 | 0.92 | 0.83 |

## Thermal Properties

Solar Absorptance= 0.92 (Ceria Doped Microsheet)

Emittance (Normal)= 0.85 (Ceria Doped Microsheet)

## Weight

84 mg/ cm² (Bare) @ 140 μm (5.5 mil) Thickness

Thickness of 175 μm typical with weight equivalence of a 140 μm thick cell.

## Temperature Coefficients

| Parameters | BOL | $1 \times 10^{15}$ (1 MeV e/cm²) |
|---|---|---|
| Jmp (μA/cm²/°C) | 6 | 14 |
| Jsc (μA/cm²/°C) | 9 | 11 |
| Vmp (mV/°C) | -6.7 | -7.2 |
| Voc (mV/°C) | -6.4 | -6.8 |

The information contained on this sheet is for reference only. Specifications subject to change without notice. 04/10/2000

## Typical IV Characteristic
AMO (135.3 mW/cm²) 28°C, Bare Cell



Voltage (V)
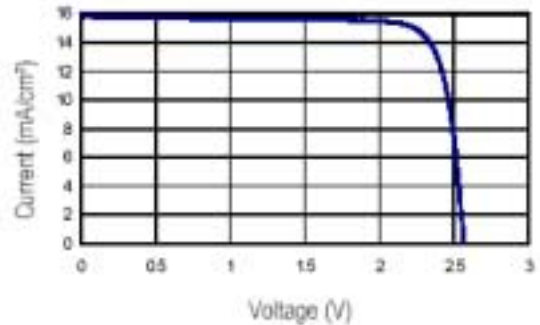


*A/R: Anti-Reflective Coating

# S P E C T R O L A B

57

THIS PAGE INTENTIONALLY LEFT BLANK

# APPENDIX B.  BEAM PROFILE PROGRAM

This appendix contains the input spread sheet for the Beam Profile program.

**Beam Profile Program**

**Inputs requested**

| | diameter(mr | sigma(mm) |
|---|---|---|
| 50% profile amp. spacing (mm) diameter (phor. screen) | 20 | 8.492569 |
| Phosphor screen from focal point (mm, **inches**) | 711.2 | 28 |
| | | |
| fluence  (e/cm2) required at device | 1.00E+15 | |
| distance device from focal point (mm, **inches**) | 2032 | 80 |
| FWHM diameter at device, sigma (mm,mm) | 55.286 | 23.475887 |
| | diameter(mr | radius(mm) |
| requested device diameter to be irradiated (**mm**) | 20 | 10 |
| | | |
| time exposure | 180 | minutes |
| | 3.00 | hours |

| | | |
|---|---|---|
| beam diameter at focal length (mm) | 1 | |
| SEM distance from focal length (mm, inches) | 381 | 15 |
| Angle of beam from screen measurement (rad,deg.) | 0.01336 | 0.76530 |
| radius of FWHM at SEM | 5.58929 | |
| ratio of target/device radius / SEM radius at FWHM | 4.946 | |

| Uniformity at Device/Target | radius (mm) | diameter (mm) |
|---|---|---|
| calculate radius for 10% down from peak on target/dev | 10.776 | 21.553 |
| calculate radius for 20% down from peak on target/dev | 15.683 | 31.366 |
| Percent down from center to target edge | 8.67% | from peak |

| | | |
|---|---|---|
| flux density (e/cm2*sec) needed on device | 9.26E+10 | |
| flux (e/sec) needed on device diameter | 2.91E+11 | |
| flux needed on SEM (e/sec) | | |
| ratio of target only flux to total flux at device | 0.0867 | 8.67% |
| total beam flux required (e/sec) | 3.35E+12 | |
| true current in beam (A) | 5.396E-07 | 5.396E-01 |
| SEM current required | 0.000E+00 | 0.000E+00 |

Instructions
1) Put in device diameter (line 10)
2) type in phosphor screen to Focal pont distance (line 4)
3) type in device to focal point distance (line 7)
4) Put in required fluence (line 6)
5) guess run time (line 12)
6) measure FWHM diameter in mm (line 3)
7) read SEM and Beam current needed

To improve uniformity place
device further from
focal point

<- Is Area>Target!!!!, if not, widen beam focus (
(place aluminum layer in)
lengthen time to check beam current down

THIS PAGE INTENTIONALLY LEFT BLANK

# APPENDIX C.  TRIPLE JUNCTION SOLAR CELL DATA PLOTS

The data contained in this appendix is the BOL and EOL IV curves for the cells under investigation in this Thesis.
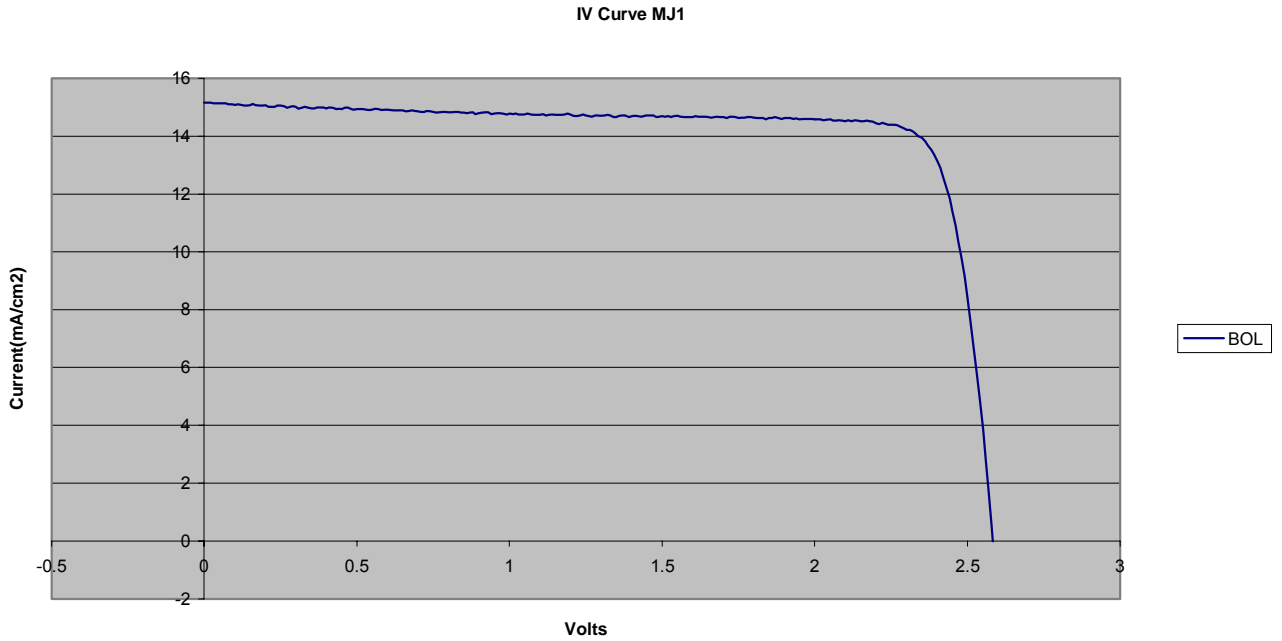
**IV Curve MJ1**



**Figure VII-1. BOL IV Curve For Test Cell 1.**
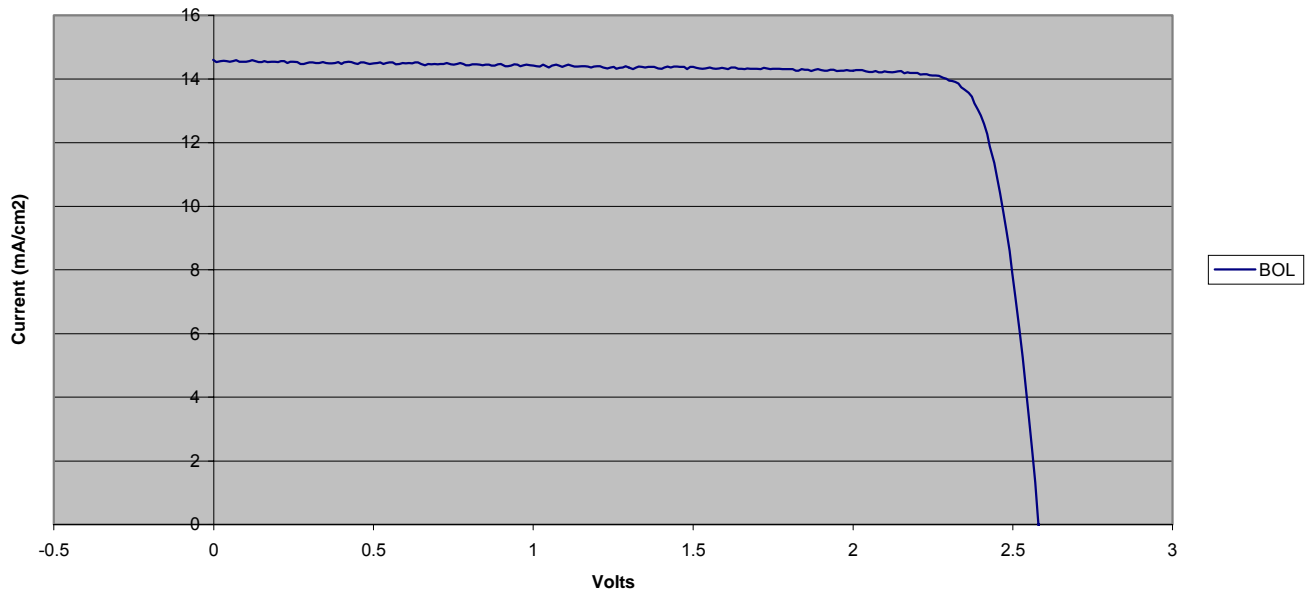


**Figure VII-2. BOL IV Curve For Test Cell 2.**
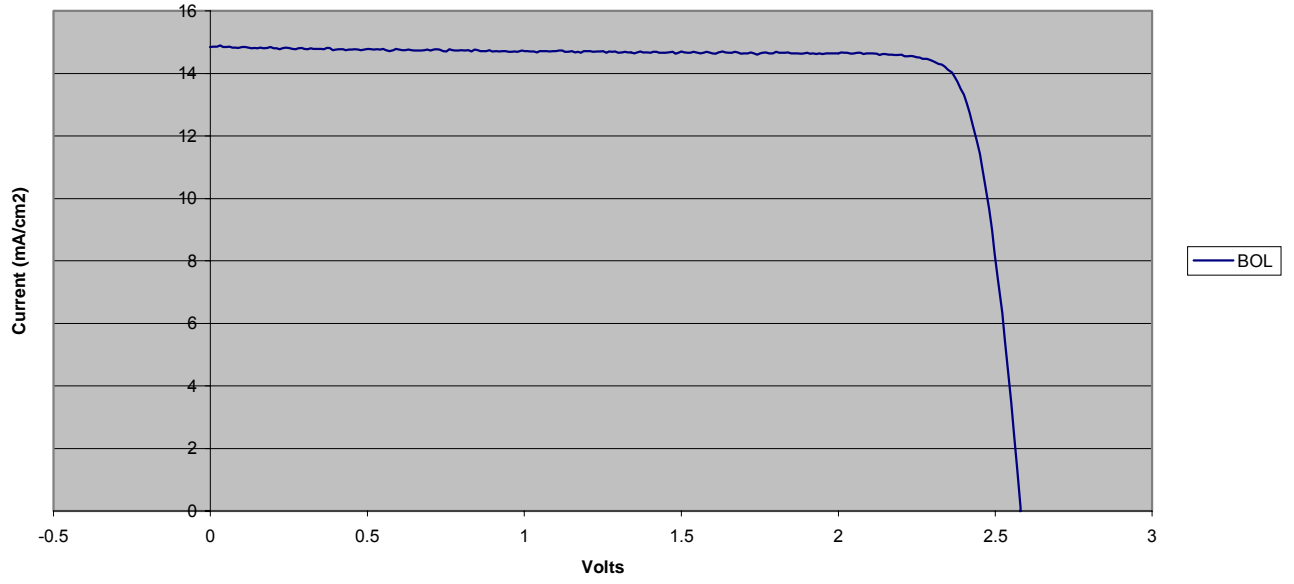
**Figure VII-3.  BOL IV Curve For Test Cell 3.**
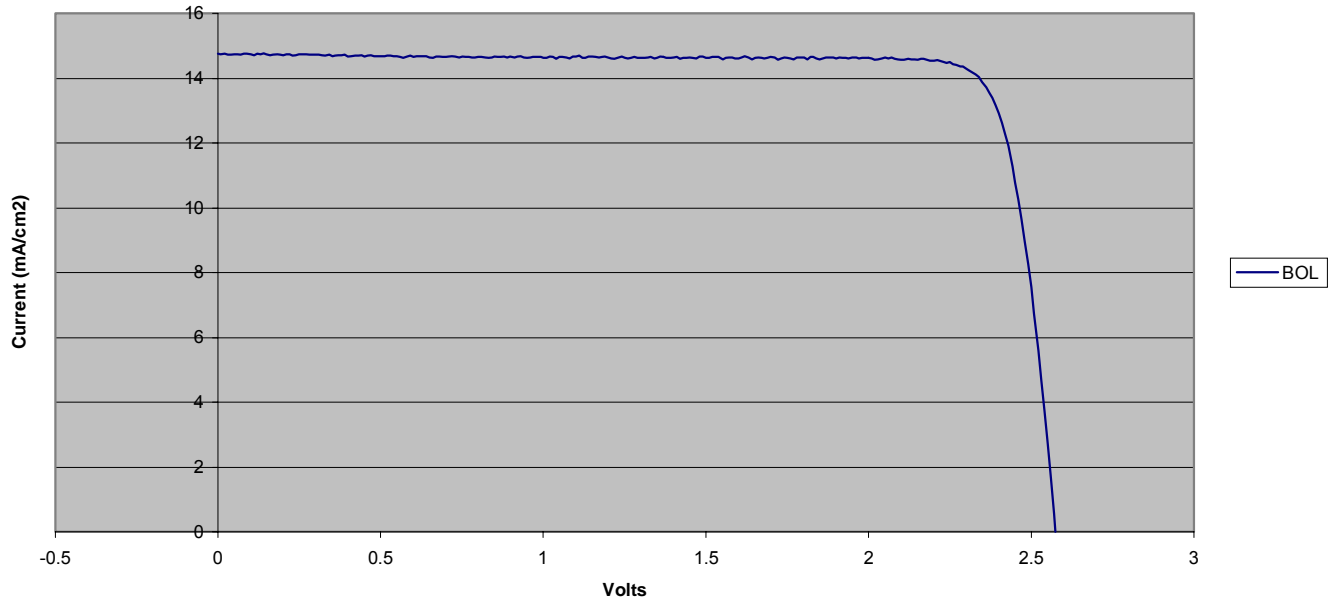
**Figure VII-4.  BOL IV Curve For Test Cell 4.**
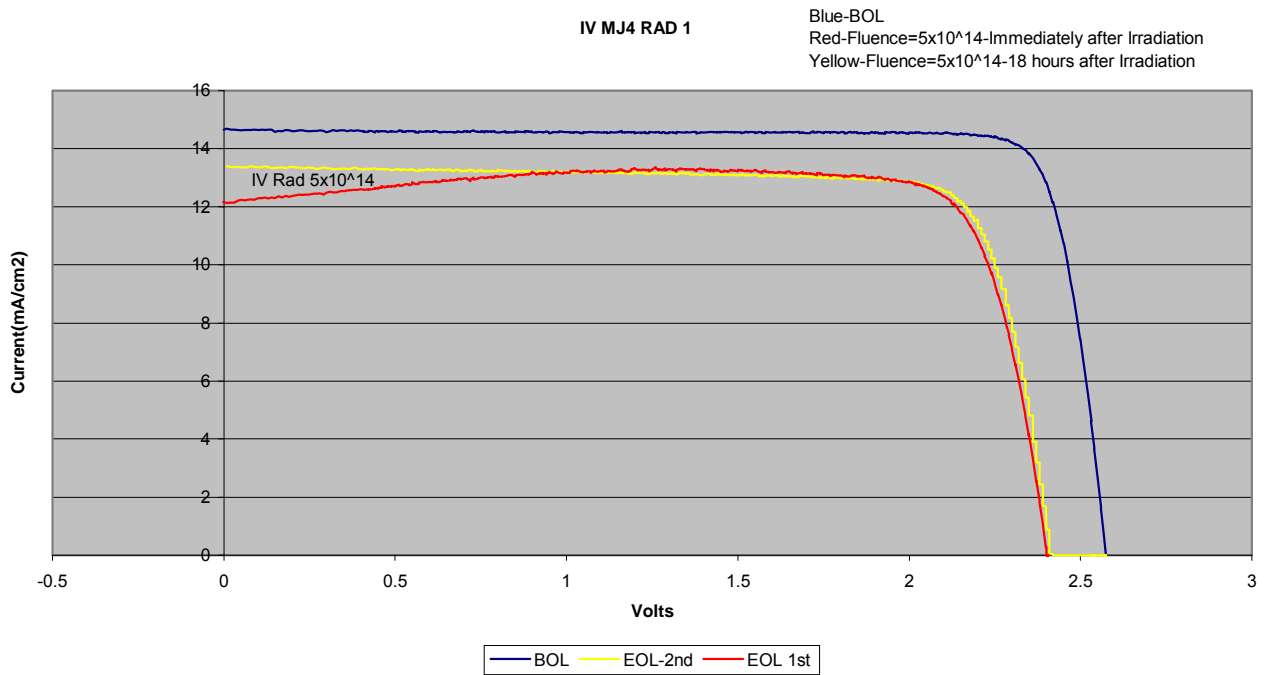
**Figure VII-5. BOL and EOL at Fluence of 5x10^14 e/cm^2**

THIS PAGE INTENTIONALLY LEFT BLANK

# LIST OF REFERENCES

1.  Tada H.Y., Carter J.R, Anspaugh B.E. & Downing R.G, " Solar Cell Radiation Handbook", 3rd Edition, JPL Publn. 82-69 (1982).

2.  C. Barnes and L. Selva, Chapter 10. Radiation Effects in MMIC Devices, JPL Publn. (1988).

3.  B. E. Anspaugh , "GaAs Solar Cell Radiation Handbook", JPL Publn. 96-9 (1996).

4.  D. C. Marvin, J.C. Nocerino, "Evaluation of Multi-Juntion Solar Cell Performance in Radiation Environments," 26th PVSC pg. 1102-1105, 2000.

5.  M.T. Barnet, W.J. Cunneen, "Design and Performance of the Electronic Linear Accelerator at the U.S. Naval Postgraduate School, Master's Thesis, Naval Postgraduate School, Monterey, California, May 1966.

6. Stanfords Linear Accelerator Virtual Vision Center, "Accelerators," [http://www2.slac.stanford.edu/vvc/accelerator.html]. May 2001.

7.  M.B. Chase, "Boto-Silicate Polycapillary Lens for Collimation of X-rays," Master's Thesis, Naval Postgraduate School, Monterey, California, June 1997.

8.  C.S. Dyer, G. R. Hopkinson, "Space Radiation Effects For Future Technologies and Missions,"QINETIQ/KI/SPACE/TR010690/1.1.

9.  Pierret R. F., Semiconductor Device Fundamentals, Addison-Wesley Publishing Company Inc., New York, NY, 1996.

10.  Singh J., "Semiconductor Band Structure," [http://www.eecs.umich.edu/~singh]. May 2001.

11.  A. Sedra, K. Smith, "MicroElectronic Circuits,"4TH ed., Oxford University Press1998.

12.  G. Li, Guohua Li, L.Peraldo Bicelli, "The Study on Composite Semiconductor Photoelectrode for High Efficiency Solar Cells," IEEE Trans 11th  QUANTSOL March14-19, 1999, Wildhaus, Switzerland.

13."SolarCells-AnOverview," [http://www.grove.ufl.edu/~kincal/documents/Solar_Cell_Basics.pdf].  May 2001.

14.  G. Wolfbauer, "The Electrochemistry of Dye Sensitized Solar Cells, their Sensitizers and their Redox Shuttle," PhD Thesis by, Monash University 1999.

15.  Guochang Li, Guohua Li, J. F. Neumark, "Investigation on ZnSe for ZnSe/GaAs/Ge High Efficiency Solar Cells," IEEE Trans 11th  QUANTSOL March14-19, 1999, Wildhaus, Switzerland.

16.  K. Emery, D. Dunlavy, H. Field, T. Moriarty, "Photovoltaic Spectral Responsivity Measurements," 2nd World Conference and Exhibition on Photovoltaic Solar Energy Conversion; 6-10 July 1998; Vienna, Austria.

17.  "Capabilities-Device Performance Spectral Responsivity  (SR) Systems," [http://emsolar.ee.tu-berlin.de/lehre/english/pv1/.]. May 2001.

18.  A. W. Bett, S. Keser, G. Stollwerck, O.V. Sulima, W. Wettling, "Over 31% Efficient GaAs/BaSb Tandem Concentrator Solar Cells," IEEE Trans. 26th PVSC pp. 931-934, Sep 30-Oct.3 1997.

19.  American Microsemiconductor, "Tunnel Diode and Back Diode," [http://www.americanmicrosemi.com/tutorials/tunneldiode.htm]. May 2001.

20.  P. R. Sharps, N. Y. Li, J. S. Hills, H. Q. Hou, "AlGaAs/InGaAIP Tunnel Junctions for Multi-Junction Solar Cells," IEEE Trans. 28TH PVC, vol. , pp. 1185-1188, Sep 2000.

21.  D.J. Friedman, J.F. Geisz, S.R. Kurtz, J.M. Olson "1-eV GaInNAs Solar Cells for Ultrahigh-Efficiency Multijunction Devices," 2nd World Conference and Exhibition on PVSEC, 6-10 July 1998, Vienna, Austria.

22.  T. Whitaker, "Lots In Space, Part 3- Solar Cells," Compound Semiconductor Magazine, Issue 4 NO. 8, November 1998.

23.  Wang, T., N. Moll, K. Cho, and J. Joannopoulos, "Computational Design of Novel Compounds for Monolithic Integration in Optoelectronics" Phys. Rev.B63, 035306 (2000).

24.  D. J. Aiken, "InGaP/GaAs/Ge Multi-junction Solar Cell Efficiency Improvements Using Epitaxial Germanium," 28th PVSC 2000.

25.  D. L. King, B. R. Hansen, J. M. Moore, D. J. Aiken, "New Methods for Measuring Performance of Monolithic Multi-junction Solar Cells," 28th PVSC 2000.

26.  P.K. Chiang, D.D. Krut and B.T. Cavicchi, "The Progress of Large Area GaInP2/GaAs/Ge triple-junction cell Development at Spectroloab," Proceeding from 14th SPRAT, October 1995.

27.  D.L. King, B.R. Hansen, J.K. Jackson, "Sandia/NIST Reference Cell Calibration Procedure," IEEE Trans. 23th PVSC pg. 1095-1101,1993.

28. J.R. Woodyard, "Laboratory Instrumentation and techniques for Characterizing Multi-Junction Solar Cells For Space Application,"16<sup>th</sup> Space Photovoltaic Research and Technology Conference, pg. 158-167, 1995.

29. NPS Space systems Academic Group, "PANSAT GaA Solar Panel Test Plan - SSAG-TP-PA006 (unpublished),"January 29, 1998.

30. S. Licht, "Multiple Band Gap Semiconductor/Electrolyte Solar Energy Conversion," J. Phys. Chem. B. 2001, 105, 6281-6294.

31. Chiang Mi University, "Linac Basics," [http://www.fnrf.science.cmu.ac.th/theory/linac/Linac%20Basic%20Concepts.html]. May 2001.

THIS PAGE INTENTIONALLY LEFT BLANK

# INITIAL DISTRIBUTION LIST

1.  Defense Technical Information Center..............................................2
    8725 John J. Kingman Rd., Suite 0944
    Ft. Belvoir, Va, 22060-6218

2.  Dudley Knox Library......................................................................2
    Naval Postgraduate School
    Monterey, Ca, 93943-5101

3.  Chairman, Code EC.........................................................................1
    Department of Electrical and Computer Engineering
    Naval Postgraduate School
    Monterey, Ca 93943-5121

4.  Professor Sherif Michael.................................................................2
    Department of Electrical and Computer Engineering
    Naval Postgraduate School
    Monterey, Ca 93943-5121

5.  Professor Ronald Pieper..................................................................1
    Department of Electrical and Computer Engineering
    Naval Postgraduate School
    Monterey, Ca 93943-5121

6.  Dan Sakoda....................................................................................1
    Department of Aeronautics and Astronautics
    Naval Postgraduate School
    Monterey, Ca 93943-5106